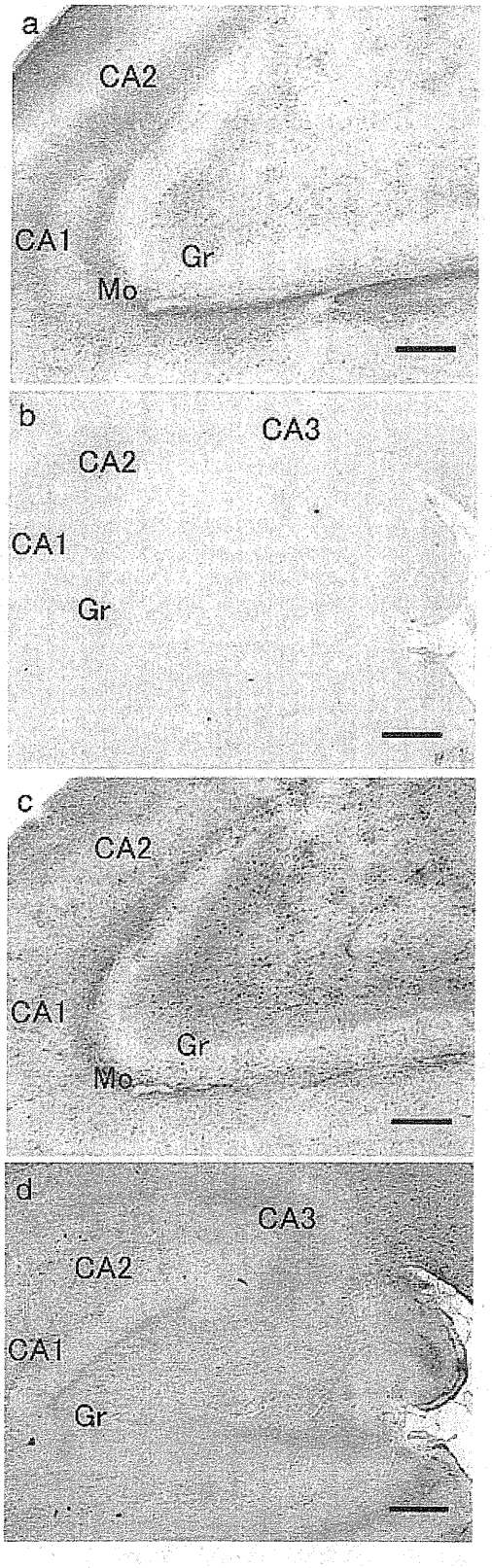


**Figure 6** Immunohistochemical staining of citrullinated proteins and PAD2. Hippocampal sections from brains of (a,c) Alzheimer's disease patients and (b,d) controls were stained for (a,b) citrullinated proteins and (c,d) PAD2 (bar, 500 μm). Gr, granule cell layer; Mo, molecular cell layer.

proposed to play a major role in hypoxic and ischemic brain injury.[39,40] Haun *et al.*[41] suggested that an influx of extra cellular calcium contributes to astroglial injury during ischemia on the basis of their experimental results with simulated ischemia in a primary culture of astrocytes. Our reports showed that PAD2 activated and citrullinated various cerebral proteins under hypoxic conditions[30] and during kainic acid-evoked neurodegeneration.[32,33] Clearly, from the weight of evidence now available, abnormal PAD activation that results in random protein citrullination could trigger the onset of neurodegenerative disease.

## Acknowledgments

This study was supported by a Grant-in-Aid for Scientific Research from the Ministry of Education, Science, and Culture, Japan (A.I.) and a grant from Health Science Research Grants for Comprehensive Research on Aging and Health supported by the Ministry of Health, Labor and Welfare, Japan (A.I.). The excellent editorial assistance of Ms P Minick is gratefully acknowledged.

## Conflicts of interest

None.

## References

1 Kubilus J, Waitkus RF, Baden HP. Partial purification and specificity of an arginine-converting enzyme from bovine epidermis. *Biochim Biophys Acta* 1980; **615**: 246–251.
2 Rogers GE, Simmonds DH. Content of citrulline and other amino acids in a protein of hair follicles. *Nature* 1958; **182**: 186–187.
3 Kubilus J, Baden HP. Purification and properties of a brain enzyme which deiminates proteins. *Biochim Biophys Acta* 1983; **745**: 285–291.
4 Ishigami A, Ohsawa T, Watanabe K, Senshu T. All-trans retinoic acid increases peptidylarginine deiminases in a newborn rat keratinocyte cell line. *Biochem Biophys Res Commun* 1996; **223**: 299–303.
5 Imparl JM, Senshu T, Graves DJ. Studies of calcineurin-calmodulin interaction: probing the role of arginine residues using peptidylarginine deiminase. *Arch Biochem Biophys* 1995; **318**: 370–377.
6 Lamensa JW, Moscarello MA. Deimination of human myelin basic protein by a peptidylarginine deiminase from bovine brain. *J Neurochem* 1993; **61**: 987–996.
7 Tarcsa E, Marekov LN, Mei G, Melino G, Lee S-C, Steinert PM. Protein Unfolding by Peptidylarginine Deiminase. Substrate specificity and structural relationships of the natural substrates trichohyalin and filaggrin. *J Biol Chem* 1996; **271**: 30709–30716.
8 Senshu T, Akiyama K, Ishigami A, Nomura K. Studies on specificity of peptidylarginine deiminase reactions using an immunochemical probe that recognizes an enzymatically deiminated partial sequence of mouse keratin K1. *J Dermatol Sci* 1999; **21**: 113–126.

9 Senshu T, Akiyama K, Kan S, Asaga H, Ishigami A, Manabe M. Detection of deiminated proteins in rat skin: probing with a monospecific antibody after modification of citrulline residues. *J Invest Dermatol* 1995; **105**: 163–169.

10 Ishigami A, Ohsawa T, Hiratsuka M *et al.* Abnormal accumulation of citrullinated proteins catalyzed by peptidylarginine deiminase in hippocampal extracts from patients with Alzheimer's disease. *J Neurosci Res* 2005; **80**: 120–128.

11 Watanabe K, Akiyama K, Hikichi K, Ohtsuka R, Okuyama A, Senshu T. Combined biochemical and immunochemical comparison of peptidylarginine deiminases present in various tissues. *Biochim Biophys Acta* 1988; **966**: 375–383.

12 Terakawa H, Takahara H, Sugawara K. Three types of mouse peptidylarginine deiminase: characterization and tissue distribution. *J Biochem (Tokyo)* 1991; **110**: 661–666.

13 Ishigami A, Kuramoto M, Yamada M, Watanabe K, Senshu T. Molecular cloning of two novel types of peptidylarginine deiminase cDNAs from retinoic acid-treated culture of a newborn rat keratinocyte cell line. *FEBS Lett* 1998; **433**: 113–118.

14 Tsuchida M, Takahara H, Minami N *et al.* cDNA nucleotide sequence and primary structure of mouse uterine peptidylarginine deiminase. Detection of a 3'-untranslated nucleotide sequence common to the mRNA of transiently expressed genes and rapid turnover of this enzyme's mRNA in the estrous cycle. *Eur J Biochem* 1993; **215**: 677–685.

15 Watanabe K, Senshu T. Isolation and characterization of cDNA clones encoding rat skeletal muscle peptidylarginine deiminase. *J Biol Chem* 1989; **264**: 15255–15260.

16 Nishijyo T, Kawada A, Kanno T, Shiraiwa M, Takahara H. Isolation and molecular cloning of epidermal- and hair follicle-specific peptidylarginine deiminase (type III) from rat. *J Biochem (Tokyo)* 1997; **121**: 868–875.

17 Rus'd AA, Ikejiri Y, Ono H *et al.* Molecular cloning of cDNAs of mouse peptidylarginine deiminase type I, type III and type IV, and the expression pattern of type I in mouse. *Eur J Biochem* 1999; **259**: 660–669.

18 Ishigami A, Asaga H, Ohsawa T, Akiyama K, Maruyama N. Peptidylarginine deiminase type I, type II, type III and type IV are expressed in rat epidermis. *Biomed Res* 2001; **22**: 63–65.

19 Guerrin M, Ishigami A, Mechin MC *et al.* cDNA cloning, gene organization and expression analysis of human peptidylarginine deiminase type I. *Biochem J* 2003; **370**: 167–174.

20 Ishigami A, Ohsawa T, Asaga H, Akiyama K, Kuramoto M, Maruyama N. Human peptidylarginine deiminase type II: molecular cloning, gene organization, and expression in human skin. *Arch Biochem Biophys* 2002; **407**: 25–31.

21 Kanno T, Kawada A, Yamanouchi J *et al.* Human peptidylarginine deiminase type III: molecular cloning and nucleotide sequence of the cDNA, properties of the recombinant enzyme, and immunohistochemical localization in human skin. *J Invest Dermatol* 2000; **115**: 813–823.

22 Nakashima K, Hagiwara T, Ishigami A *et al.* Molecular characterization of peptidylarginine deiminase in HL-60 cells induced by retinoic acid and 1alpha,25-dihydroxyvitamin D(3). *J Biol Chem* 1999; **274**: 27786–27792.

23 Chavanas S, Mechin MC, Takahara H *et al.* Comparative analysis of the mouse and human peptidylarginine deiminase gene clusters reveals highly conserved non-coding segments and a new human gene, PADI6. *Gene* 2004; **330**: 19–27.

24 Asaga H, Nakashima K, Senshu T, Ishigami A, Yamada M. Immunocytochemical localization of peptidylarginine deiminase in human eosinophils and neutrophils. *J Leukocyte Biol* 2001; **70**: 46–51.

25 Baden HP, Kubilus J. The growth and differentiation of cultured newborn rat keratinocytes. *J Invest Dermatol* 1983; **80**: 124–130.

26 Ishigami A, Asaga H, Ohsawa T, Akiyama K, Maruyama N. Protein deimination and peptidylarginine deiminase expression during cornification of rat epidermal keratinocytes. *Biomed Res* 2002; **23**: 145–151.

27 Resing KA, al-Alawi N, Blomquist C, Fleckman P, Dale BA. Independent regulation of two cytoplasmic processing stages of the intermediate filament-associated protein filaggrin and role of Ca2+ in the second stage. *J Biol Chem* 1993; **268**: 25139–25145.

28 Keller JN, Hanni KB, Markesbery WR. Impaired proteasome function in Alzheimer's disease. *J Neurochem* 2000; **75**: 436–439.

29 Maccioni RB, Munoz JP, Barbeito L. The molecular bases of Alzheimer's disease and other neurodegenerative disorders. *Arch Med Res* 2001; **32**: 367–381.

30 Asaga H, Ishigami A. Protein deimination in the rat brain: generation of citrulline-containing proteins in cerebrum perfused with oxygen-deprived media. *Biomed Res* 2000; **21**: 197–205.

31 Vincent SR, Leung E, Watanabe K. Immunohistochemical localization of peptidylarginine deiminase in the rat brain. *J Chem Neuroanat* 1992; **5**: 159–168.

32 Asaga H, Ishigami A. Protein deimination in the rat brain after kainate administration: citrulline-containing proteins as a novel marker of neurodegeneration. *Neurosci Lett* 2001; **299**: 5–8.

33 Asaga H, Akiyama K, Ohsawa T, Ishigami A. Increased and type II-specific expression of peptidylarginine deiminase in activated microglia but not hyperplastic astrocytes following kainic acid-evoked neurodegeneration in the rat brain. *Neurosci Lett* 2002; **326**: 129–132.

34 Akiyama K, Sakurai Y, Asou H, Senshu T. Localization of peptidylarginine deiminase type II in a stage-specific immature oligodendrocyte from rat cerebral hemisphere. *Neurosci Lett* 1999; **274**: 53–55.

35 Senshu T, Sato T, Inoue T, Akiyama K, Asaga H. Detection of citrulline residues in deiminated proteins on polyvinylidene difluoride membrane. *Anal Biochem* 1992; **203**: 94–100.

36 Asaga H, Senshu T. Combined biochemical and immunocytochemical analyses of postmortem protein deimination in the rat spinal cord. *Cell Biol Int* 1993; **17**: 525–532.

37 Katzman R. Alzheimer's disease. *N Engl J Med* 1986; **314**: 964–973.

38 Smith MA. Alzheimer disease. *Int Rev Neurobiol* 1998; **42**: 1–54.

39 Hossmann KA. The hypoxic brain. Insights from ischemia research. *Adv Exp Med Biol* 1999; **474**: 155–169.

40 Choi DW. Calcium-mediated neurotoxicity: relationship to specific channel types and role in ischemic damage. *Trends Neurosci* 1988; **11**: 465–469.

41 Haun SE, Murphy EJ, Bates CM, Horrocks LA. Extracellular calcium is a mediator of astroglial injury during combined glucose-oxygen deprivation. *Brain Res* 1992; **593**: 45–50.

Biomedical Research 30 (4) 227-233, 2009

# Elevated levels of 4-hydroxynonenal-histidine Michael adduct in the hippocampi of patients with Alzheimer's disease

Mitsugu FUKUDA[1], Fumihisa KANOU[2], Nobuko SHIMADA[1], Motoji SAWABE[3], Yuko SAITO[3, 4], Shigeo MURAYAMA[4], Masakatsu HASHIMOTO[2], Naoki MARUYAMA[1] and Akihito ISHIGAMI[1, 5]

[1] Aging Regulation, Tokyo Metropolitan Institute of Gerontology, Tokyo, Japan; [2] Shima Laboratories, Tokyo, Japan; [3] Department of Pathology, Tokyo Metropolitan Geriatric Hospital, Tokyo, Japan; [4] Department of Neuropathology, Tokyo Metropolitan Institute of Gerontology, Tokyo, Japan; and [5] Department of Biochemistry, Faculty of Pharmaceutical Sciences, Toho University, Chiba, Japan

*(Received 7 May 2009; and accepted 12 June 2009)*

## ABSTRACT

Alzheimer's disease (AD) is among the most common causes of progressive cognitive impairment in humans and is characterized by neurodegeneration in the brain. Lipid peroxidation is thought to play a role in the pathogenesis of AD. 4-hydroxynonenal (HNE) results from peroxidation of polyunsaturated fatty acids and it in turn gives evidence of lipid peroxidation *in vivo*. HNE reacts with protein histidine residue to form a stable HNE-histidine Michael adduct. To clarify the influence of lipid peroxidation on the pathogenesis of AD, we measured HNE-histidine Michael adduct in hippocampi from four AD patients and four age-matched controls by means of semiquantitative immunohistochemistry using a specific antibody to cyclic hemiacetal type of HNE-histidine Michael adduct. This antibody does not react with the ring-opened form of HNE-histidine Michael adduct and the pyrrole form of HNE-lysine Michael adduct. The HNE adduct was detected in the hippocampi of both AD and control donors, especially in the CA2, CA3 and CA4 sectors. Immunoreactive intensity of HNE adduct in these sectors were significantly higher in AD patients than in the controls. The HNE adduct was found in the perikarya of pyramidal cells in the hippocampus. These results show that the hippocampi of patients with AD undergo lipid peroxidation and imply that this activity underlies the production of cytotoxic products such as HNE that are responsible for the pathogenesis of AD.

The progressive cognitive impairment of Alzheimer's disease (AD) is associated with neuronal loss as well as the formation of neurofibrillary tangles (NFTs) and senile plaques in the brain (25). Free radical-mediated oxidative damage, energy depletion, deposition of amyloids and NFTs, excitotoxicity, and vascular endothelial cell damage are all thought to participate in the pathogenesis of AD (13). Oxygen-derived free radicals, byproducts of respiration, cause oxidative damage to cellular biomolecules including lipids, proteins and nucleic acids. The brain seems to be especially vulnerable to lipid peroxidation by free radicals, because it consumes approximately one-fifth of humans' oxygen intake, has a relative paucity of antioxidant systems and contains high concentrations of polyunsaturated fatty acids (PUFAs) (11). Lipid peroxidation results in structural damage to membranes and generation of secondary products such as reactive aldehydes

Address correspondence to: Akihito Ishigami, Ph.D. Department of Biochemistry, Faculty of Pharmaceutical Sciences, Toho University, Miyama 2-2-1, Funabashi, Chiba 274-8510, Japan
Tel/Fax: +81-47-472-1536
E-mail: ishigami@phar.toho-u.ac.jp

Abbreviations used: AD, Alzheimer's disease; DAB, 3,3'-diaminobenzidine tetrahydrochloride; HNE, 4-hydroxynonenal; MAP2, microtubule-associated protein 2; NFT, neurofibrillary tangle; PBS, phosphate buffered saline; PUFAs, polyunsaturated fatty acids.

that modify proteins and nucleic acids (5). Therefore, as reported, lipid peroxidation in the brains of AD patients not only harms cells but increases levels of such peroxidation products as thiobarbituric acid-reactive substances (10), acrolein-deoxyguanosine adducts (9), and cytotoxic compounds such as acrolein (12) and 4-hydroxynonenal (HNE) (17).

Lipid peroxidation propagates itself by autoxidation initiated by free radicals and produces considerable amounts of secondary products before the process terminates (21). These well-known secondary products include reactive aldehydes, such as acrolein, malondialdehyde, HNE, and 4-hydroxyhexenal (5). HNE is product that results from the lipid peroxidation of n-6 PUFAs, *e.g.,* linoleic acid and arachidonic acid (5). Because the brain is rich in arachidonic acid (29), lipid peroxidation tends to produce HNE at that site. These substances then react with proteins, nucleic acids and small molecules such as glutathione in cells and eventually impair normal biological functions of the essential components (5). Indeed, HNE is cytotoxic for cultured neuronal cells (2, 5, 8, 15). Therefore, HNE might induce neuronal cell death and neurodegeneration in patients with AD.

Measuring the exact quantity of HNE *in vivo* is difficult, since they are rapidly consumed when their chemically active aldehyde reacts with such cellular components as glutathione, proteins and nucleic acids (5). HNE reacts with lysine, histidine and cysteine residues in proteins to form Michael adducts and also Schiff base products (lysine ε-$NH_2$). When HNE reacts with proteins, HNE-histidine Michael adduct is a major product that develops in the cyclic hemiacetal form (3, 27). Because the cyclic hemiacetal form of HNE is relatively stable (5), the detection of HNE Michael adduct is considered a reliable index of lipid peroxidation. This property enabled us to measure HNE-histidine Michael adduct using the specific antibody to cyclic hemiacetal type of HNE-histidine Michael adduct.

To clarify the influence of lipid peroxidation on the pathogenesis of AD, we directly assessed the cyclic hemiacetal type of HNE-histidine Michael adduct in brain specimens from AD subjects and age-matched controls. As a result, the HNE adduct was detected in the hippocampi of both groups, especially the CA2, CA3 and CA4 sectors. The important difference was significantly higher levels of the HNE adduct in the brains of patients with AD. This is the first report of specific antibody usage for direct detection of HNE-histidine Michael adduct in the cyclic hemiacetal form within hippocampi from humans with AD.

## MATERIALS AND METHODS

*Human subjects.* All clinical data from patients and information at autopsies from four patients with AD (two women and two men) and four (one women and three men) normal (no AD), age-matched subjects who died during the last several decades were retrieved from the autopsy database of the Department of Tokyo Metropolitan Geriatric Hospital, Tokyo, Japan. Brain specimens were registered in the Brain Bank for Aging Research (BBAR) organized by Tokyo Metropolitan Geriatric Hospital and Tokyo Metropolitan Institute of Gerontology (TMIG). Brain specimens used in this study were from patients clinically diagnosed as having AD-positive and control subjects without any sign of AD. All AD patients met accepted criteria for the neuropathologic diagnosis of AD based on the National Institute of Aging (NIA)-Reagan Institute Criteria for the Neuropathological Diagnosis of AD (1997) (1), combining abundant neuritic plaques in the neocortex (definite AD with consortium to establish a registry for AD criteria) and a profusion of NFTs in the limbic and neocortical areas (Braak and Braak staging, VI). Normal subjects used as controls were individuals with no history of dementia or other neurological disorders. Neuropathologic evaluation of control brains revealed only age-associated gross and histopathologic alterations (Braak and Braak NFT staging, I and SP stage, 0 or A). The subjects' demographic data are summarized in Table 1. The human studies were approved by Ethics Committees of TMIG and the Tokyo Metropolitan Geriatric Hospital.

*Immunohistochemistry.* Specimens were taken from the hippocampus and fixed with 4% paraformaldehyde in this study. Paraffin-embedded hippocampal sections were deparaffinized, rehydrated with xylene, alcohol and phosphate buffered saline (PBS), microwaved for 5 min in boiling 10 mM citrate buffer, pH 6.0, and immersed in 3% $H_2O_2$ in methanol for 15 min to reduce endogenous peroxidase activity. After blocking treatment with 10% non-immune goat serum in PBS (blocking solution) for 60 min at room temperature, the specimens were incubated with the primary antibodies overnight at 4°C and then for 60 min at room temperature. Mouse monoclonal antibody against HNE-histidine Michael adduct which was specific for their cyclic hemiacetal form was purchased from NOF Corporation (Tokyo,

Japan), and was used at a dilution of 1 : 100 with a blocking solution. After adequate washing with PBS, specimens were incubated with the secondary antibody (goat anti-mouse IgG conjugated with horseradish peroxidase, Simplestain MAX-PO (M); Nichirei Biosciences Inc., Tokyo, Japan) for 60 min at room temperature. Thorough washing with PBS and incubation with 0.02% 3,3'-diaminobenzidine tetrahydrochloride (DAB) (Wako Pure Chemical Industries, Osaka, Japan) followed for 10 min at room temperature to visualize HNE-adduct. For double-labeling immunohistochemistry, two primary antibodies were used: anti-microtubule-associated protein 2 (MAP2) and the anti-HNE-histidine adduct antibodies. Tissue specimens were incubated with the anti-MAP2 antibody (1 : 500 dilution; Chemicon AB5622, rabbit polyclonal antibody; Billerica, MA, USA) to confirm pyramidal neurons, and then with Simplestain AP (R) as a secondary antibody conjugated with alkaline phosphatase. The alkaline phosphatase activity was visualized with Vector Red Alkaline Phosphatase Substrate Kit I (Vector Laboratories, Burlingame, CA, USA). Subsequently, the specimens were incubated with the anti-HNE adduct antibody as mentioned above. Hematoxylin was used for counter staining. The antibody used against HNE-histidine Michael adduct is specific for their cyclic hemiacetal form and does not react with the ring-opened form of HNE-histidine Michael adduct and the pyrrole form of HNE-lysine Michael adduct (26).

The four hippocampal sectors (CA1 through CA4) were delineated and cells that had a large nucleus containing a clearly visible nucleolus in these sectors were referred to pyramidal cells according to the description of Mani *et al.* (14). Immunoreactive intensity of the HNE-Michael adduct was assessed by measuring 20 fields of hippocampal sectors in the specimens under a 40 × objective microscopic field. The extent of staining intensity in pyramidal cells was classified into the following two grades: Pyr-small (small staining size less than half of the pyramidal cell nucleus) and Pyr-large (large staining size more than half of the pyramidal cell nucleus). The extent of staining intensity in non-pyramidal cells was also classified into the following two grades: Non-small (small staining size less than the cell nuclei) and Non-large (large staining size more than the cell nuclei). The percent ratio of these grades in each sector was calculated by following formulation: percent of Pyr-small = (numbers of Pyr-small grade / (numbers of Pyr-small grade + Pyr-large grade)) × 100; percent of Pyr-large = (numbers of Pyr-large grade / (numbers of Pyr-small grade + Pyr-large grade)) × 100; percent of Non-small = (numbers of Non-small grade / (numbers of Non-small grade + Non-large grade)) × 100; and percent of Non-large = (numbers of Non-large grade / (numbers of Non-small grade + Non-large grade)) × 100.

*Statistical analysis.* The results are expressed as mean ± SEM. Statistical analyses were conducted by using Graphpad Prism 4 software (version 4.0, Graphpad Software Inc., San Diego, CA, USA). Significance was defined as a $P$ value less than 0.05.

## RESULTS

*Clinical features of subjects*

The subjects' demographic data are summarized in Table 1. The mean ages of the AD group and the control group were 86 and 78 years, respectively, and there was no significant difference between these two groups (*t-test*, two-sided). Neither brain weight, gender, nor postmortem interval differed significantly between the two groups according to a *t-test* (two-sided), Fisher's exact test, or *t-test* (two-sided), respectively.

*HNE Michael adduct in the hippocampi from AD patients and non-AD controls*

HNE Michael adduct in the hippocampi was detected in all specimens from both AD and controls. Especially, CA2–4 sectors contained an abundance of the HNE adduct compared with the adjacent CA1 sector (Fig. 1B and Table 2).

HNE Michael adduct immunoreactivity was seen

**Table 1** *Demographic data for AD subjects and controls*

| | Age (yr) | PMI (h) | Gender | BW (g) | Braak stage | |
|---|---|---|---|---|---|---|
| | | | | | NFT | SP |
| AD | 86 ± 3 | 10.0 ± 0.1 | 2 M/2 F | 1,110 ± 52 | VI (4) | C (4) |
| Controls | 78 ± 2 | 4.4 ± 2.5 | 3 M/1 F | 1,241 ± 67 | I (4) | 0 (4) |

Data are expressed as mean ± SEM. Parentheses indicate the number of subject. AD, Alzheimer disease; PMI, postmortem interval; h, hour; BW, brain weight; g, gram; yr, year; NFT, neurofibrillary tangle; SP, senile plaque

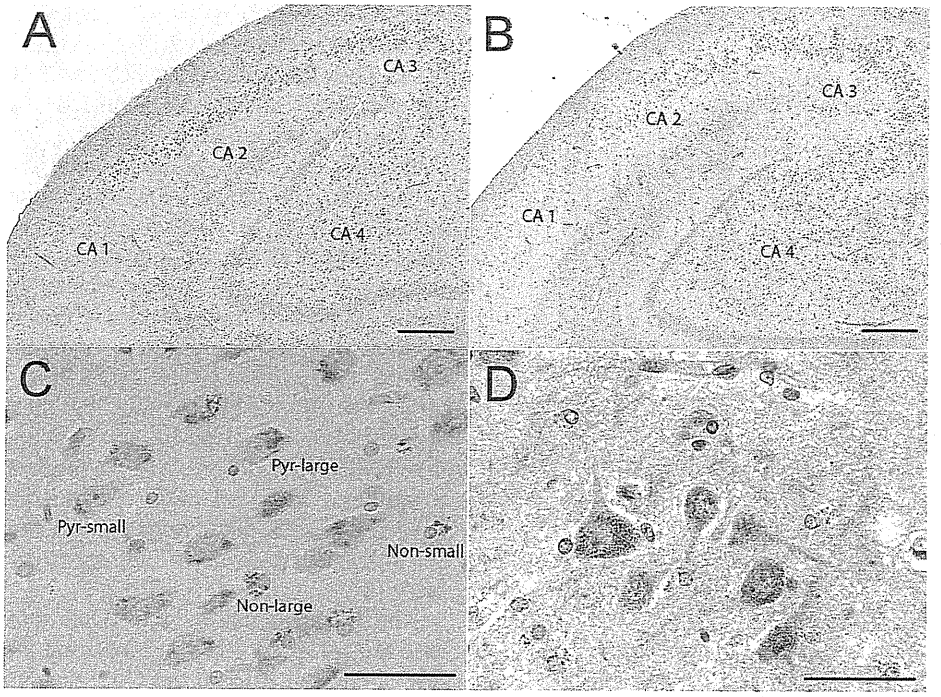


**Fig. 1** Representative photomicrographs of immunostaining for HNE-Michael adduct in the hippocampus. HNE-Michael adduct in the hippocampi of AD (A, C, D) and non-AD control (B) and MAP2 (D) are visualized using DAB (brown) and Vector Red (pink), respectively. Counter staining was performed with hematoxylin. Substances with immunoreactivity to anti-HNE-histidine Michael adduct are seen in pyramidal cells as a granular form (C, D) and seen in non-pyramidal cells as amorphous deposits (C). For statistical analysis, the extent of staining intensity of the HNE adduct is classified into two grades (Pyr-small and Pyr-large) for the pyramidal cells, and two grades (Non-small and Non-large) for the non-pyramidal cells, as described in Materials and Methods. Bar = 50 μm (A and B) and 5 μm (C and D).

**Table 2** *Immunostaining intensity of the HNE-Michael adduct in the hippocampus*

| Sector | Case | Pyramidal cells | | | Non-pyramidal cells | | |
|---|---|---|---|---|---|---|---|
| | | Pyr-small | Pyr-large | *P* value | Non-small | Non-large | *P* value |
| CA1 | AD | 228 | 39 | | 126 | 95 | |
| | Control | 433 | 25 | < 0.0001 | 143 | 125 | NS |
| CA2/3 | AD | 168 | 433 | | 236 | 463 | |
| | Control | 296 | 425 | < 0.0001 | 177 | 255 | 0.0157 |
| CA4 | AD | 42 | 238 | | 177 | 299 | |
| | Control | 206 | 364 | < 0.0001 | 205 | 223 | 0.0012 |

Staining intensity of the HNE adduct is classified into two grades (Pyr-small and Pyr-large) for the pyramidal cells, and two grades (Non-small and Non-large) for the non-pyramidal cells, as described in Materials and Methods. Fisher's exact test; NS, not significant.

as intracellular accumulations within pyramidal cells in the hippocampi of AD and controls (indicated in brown in Fig. 1C and D). In addition to the criteria of pyramidal cells in Materials and Methods, pyramidal cells were also confirmed by anti-MAP2 antibody as shown in Fig. 1D. The HNE adduct seemed to be composed of a mass of granular substances localized in the perikarya of pyramidal cells in the hippocampus, especially at the CA2, CA3 and CA4 sectors (Fig. 1C and D). Notably, the staining intensity for HNE Michael adduct was far stronger in these sectors of the AD brain samples than in those of the controls (Table 2, Fisher's exact test: $P < 0.0001$). Similarly, the ratio of the severe grade indicated as Pyr-large was relatively higher in the CA2/3 and CA4 sectors of AD patients compared with controls (Fig. 2A).

Additionally, a large amount of amorphous HNE

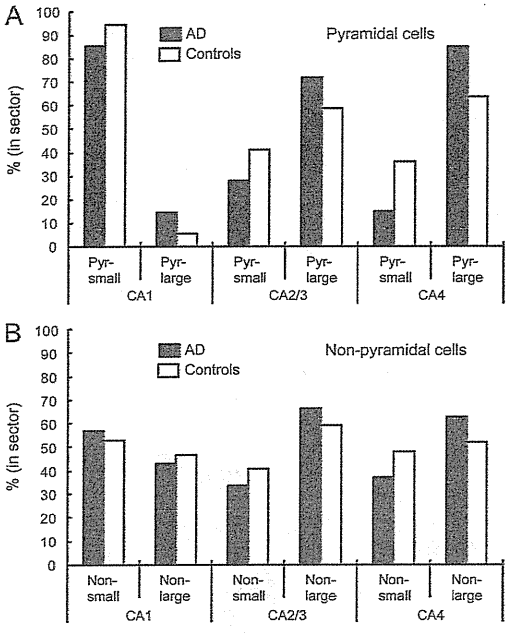


**Fig. 2** Ratio of immunostaining intensity of the HNE-Michael adduct in the hippocampal sectors. Immunostaining intensity of the HNE-Michael adduct was assessed as described in Materials and Methods. Percent of the grades of HNE staining intensity in each sector was calculated as described in Materials and Methods. (A), pyramidal cells; (B), non-pyramidal cells; closed bars, AD; open bars, age-matched controls. The percent ratio of the Pyr-large grade of the pyramidal cells and the percent ratio of the Non-large grade of the non-pyramidal cells are relatively higher in the CA2/3 and CA4 sectors of AD patients compared with controls.

Michael adduct was seen around the nuclei of non-pyramidal cells other than the pyramidal cells in the hippocampus, and this material was referred to as non-pyramidal cell deposits (abbreviated as Non-small and Non-large in Fig. 1C). Numerous non-pyramidal cell deposits were found in the CA2, CA3 and CA4 sectors of the hippocampi from AD and controls (Table 2), but the staining intensity of these deposits again differed significantly in the two groups (Table 2, Fisher's exact test: $P < 0.02$). That is, the ratio of large amorphous deposits (Non-large grade in Table 2) to total deposits was relatively higher in these sectors of the AD tissue compared with that from age-matched controls (Fig. 2B).

## DISCUSSION

Here, we found an intracellular accumulation of HNE-histidine Michael adduct in pyramidal cells of the hippocampus, most notably at the CA2, CA3 and CA4 sectors by using a specific antibody to cyclic hemiacetal type of HNE-histidine Michael adduct. This antibody does not react with the ring-opened form of HNE-histidine Michael adduct and the pyrrole form of HNE-lysine Michael adduct (26). Although the HNE adduct occupied hippocampi from both AD and age-matched, non-AD controls, significantly larger quantities of the HNE adduct were present in the CA2–4 sectors of AD patients than those of controls. These results show that pyramidal neurons in these sectors within hippocampi of persons with AD are prone to undergo lipid peroxidation. Consequently, increased lipid peroxidation might be responsible for the neuronal degeneration and death characteristic of AD. In support is the fact that HNE, a lipid peroxidation product is cytotoxic to cultured neuronal cells via impairment of $Na^+$, $K^+$-ATPase (15), disruptions of microtubule structure (7, 20), caspase-3 activation, and cytochrome c release (6).

The distribution of the HNE adduct differed among CA sectors in the hippocampus. Although a few pyramidal cells in the CA1 sector contained the HNE adduct, a great number of cells in the CA2–4 sectors contained massive amounts of the HNE adduct. A similar spatial distribution pattern was found for malondialdehyde-conjugated proteins identified in persons with AD and age-matched controls (4). Thus, these results suggest that pyramidal cells in the CA1 sector might resist lipid peroxidation. On the other hand, after sodium borohydride treatment, the ring-opened form of HNE-histidine Michael adduct was seen frequently in hippocampi of AD patients but rarely in age-matched controls, and in the former case the percentage of immunoreactive pyramidal cells in the CA1 sector was comparable to that of the CA2–4 sectors (19). That result disagrees with the outcome presented here, possibly because antibodies of differing specificities were used in the two studies. That is, the previously used antibody against the ring-opened form of HNE-histidine Michael adduct rarely stained hippocampi from control subjects, whereas the antibody used in this study stained hippocampal tissues from controls and AD patients to comparable extents.

We also showed that amorphous deposits immunoreactive to the anti-HNE adduct antibody in non-pyramidal cells were significantly increased in the CA2–4 sectors of hippocampal samples from AD patients compared with age-matched control. These deposits were found around small nuclei in the CA2–4 sectors of hippocampal samples. Although the all cell types containing these small nuclei were

not identified, some cells were positively stained with glial fibrillary acidic protein which is an astrocyte marker protein but not all cells. Immunoreactivity similar to the amorphous staining described here was seen in astrocytes when using antibody against the ring-opened form of HNE-histidine Michael adduct (19) and antibody against malondialdehyde-conjugated proteins (4). Therefore, the cells containing the small nuclei we viewed around amorphous deposits could be astrocytes.

In addition to the cyclic hemiacetal form and the ring-opened form of HNE-histidine Michael adduct, the pyrrole form of HNE-lysine Michael adduct (18, 24) was detected in the hippocampus (24) and entorhinal cortex (18) of samples from AD patients by using specific antibodies. Other than the immunohistochemical detection of HNE-conjugated proteins, elevated levels of HNE itself (17, 28) and isoprostanes (16, 22, 23), stable products derived from lipid peroxidation of PUFAs, these reports confirm increased lipid peroxidation in the brains of AD compared with control individuals. Thus, our results and those studies provide firm evidence of increased lipid peroxidation in brains that manifest AD.

Here we have documented strong evidence of lipid peroxidation in the hippocampi of both AD patients and age-matched, non-AD controls by identifying the presence of the HNE adduct. Presumably, the increased levels of HNE adduct in the hippocampi of AD patients signifies that the brains of such patients with AD tend to be more sensitive to lipid peroxidation than normal brains. In that environment, accelerated lipid peroxidation might play a pivotal role in the pathogenesis of AD by producing HNE and/or other cytotoxic products.

## Acknowledgements

This study is supported by a Grant-in-Aid for Scientific Research from the Ministry of Education, Science, and Culture, Japan (to A.I., S.H. and N.S.) and a grant from Health Science Research Grants for Comprehensive Research on Aging and Health supported by the Ministry of Health Labor and Welfare, Japan (to A.I.). We thank Ms. Eiko Moriizumi for her technical advices on immunohistochemistry. We also thank Ms. P. Minick for the excellent English editorial assistance.

## REFERENCES

1. Consensus recommendations for the postmortem diagnosis of Alzheimer's disease (1997). The National Institute on Aging, and Reagan Institute Working Group on Diagnostic Criteria for the Neuropathological Assessment of Alzheimer's Disease. *Neurobiol Aging* **18**, S1–2.
2. Abdul HM and Butterfield DA (2007) Involvement of PI3K/PKG/ERK1/2 signaling pathways in cortical neurons to trigger protection by cotreatment of acetyl-L-carnitine and alpha-lipoic acid against HNE-mediated oxidative stress and neurotoxicity: implications for Alzheimer's disease. *Free Radic Biol Med* **42**, 371–384.
3. Amarnath V, Valentine WM, Montine TJ, Patterson WH, Amarnath K, Bassett CN and Graham DG (1998) Reactions of 4-hydroxy-2(E)-nonenal and related aldehydes with proteins studied by carbon-13 nuclear magnetic resonance spectroscopy. *Chem Res Toxicol* **11**, 317–328.
4. Dei R, Takeda A, Niwa H, Li M, Nakagomi Y, Watanabe M, Inagaki T, Washimi Y, Yasuda Y, Horie K, Miyata T and Sobue G (2002) Lipid peroxidation and advanced glycation end products in the brain in normal aging and in Alzheimer's disease. *Acta Neuropathol* **104**, 113–122.
5. Esterbauer H, Schaur RJ and Zollner H (1991) Chemistry and biochemistry of 4-hydroxynonenal, malonaldehyde and related aldehydes. *Free Radic Biol Med* **11**, 81–128.
6. Ji C, Amarnath V, Pietenpol JA and Marnett LJ (2001) 4-hydroxynonenal induces apoptosis via caspase-3 activation and cytochrome c release. *Chem Res Toxicol* **14**, 1090–1096.
7. Kokubo J, Nagatani N, Hiroki K, Kuroiwa K, Watanabe N and Arai T (2008) Mechanism of destruction of microtubule structures by 4-hydroxy-2-nonenal. *Cell Struct Funct* **33**, 51–59.
8. Kruman I, Bruce-Keller AJ, Bredesen D, Waeg G and Mattson MP (1997) Evidence that 4-hydroxynonenal mediates oxidative stress-induced neuronal apoptosis. *J Neurosci* **17**, 5089–5100.
9. Liu X, Lovell MA and Lynn BC (2005) Development of a method for quantification of acrolein-deoxyguanosine adducts in DNA using isotope dilution-capillary LC/MS/MS and its application to human brain tissue. *Anal Chem* **77**, 5982–5989.
10. Lovell MA, Ehmann WD, Butler SM and Markesbery WR (1995) Elevated thiobarbituric acid-reactive substances and antioxidant enzyme activity in the brain in Alzheimer's disease. *Neurology* **45**, 1594–1601.
11. Lovell MA and Markesbery WR (2007) Oxidative damage in mild cognitive impairment and early Alzheimer's disease. *J Neurosci Res* **85**, 3036–3040.
12. Lovell MA, Xie C and Markesbery WR (2001) Acrolein is increased in Alzheimer's disease brain and is toxic to primary hippocampal cultures. *Neurobiol Aging* **22**, 187–194.
13. Mamelak M (2007) Alzheimer' s disease, oxidative stress and gammahydroxybutyrate. *Neurobiol Aging* **28**, 1340–1360.
14. Mani RB, Lohr JB and Jeste DV (1986) Hippocampal pyramidal cells and aging in the human: a quantitative study of neuronal loss in sectors CA1 to CA4. *Exp Neurol* **94**, 29–40.
15. Mark RJ, Lovell MA, Markesbery WR, Uchida K and Mattson MP (1997) A role for 4-hydroxynonenal, an aldehydic product of lipid peroxidation, in disruption of ion homeostasis and neuronal death induced by amyloid beta-peptide. *J Neurochem* **68**, 255–264.
16. Markesbery WR, Kryscio RJ, Lovell MA and Morrow JD (2005) Lipid peroxidation is an early event in the brain in amnestic mild cognitive impairment. *Ann Neurol* **58**, 730–735.
17. Markesbery WR and Lovell MA (1998) Four-hydroxynonenal, a product of lipid peroxidation, is increased in the brain in Alzheimer's disease. *Neurobiol Aging* **19**, 33–36.

18. Montine KS, Olson SJ, Amarnath V, Whetsell WO, Jr., Graham DG and Montine TJ (1997) Immunohistochemical detection of 4-hydroxy-2-nonenal adducts in Alzheimer's disease is associated with inheritance of APOE4. *Am J Pathol* **150**, 437–443.
19. Montine KS, Reich E, Neely MD, Sidell KR, Olson SJ, Markesbery WR and Montine TJ (1998) Distribution of reducible 4-hydroxynonenal adduct immunoreactivity in Alzheimer disease is associated with APOE genotype. *J Neuropathol Exp Neurol* **57**, 415–425.
20. Neely MD, Sidell KR, Graham DG and Montine TJ (1999) The lipid peroxidation product 4-hydroxynonenal inhibits neurite outgrowth, disrupts neuronal microtubules, and modifies cellular tubulin. *J Neurochem* **72**, 2323–2333.
21. Porter NA, Caldwell SE and Mills KA (1995) Mechanisms of free radical oxidation of unsaturated lipids. *Lipids* **30**, 277–290.
22. Pratico D, V MYL, Trojanowski JQ, Rokach J and Fitzgerald GA (1998) Increased F2-isoprostanes in Alzheimer's disease: evidence for enhanced lipid peroxidation in vivo. *FASEB J* **12**, 1777–1783.
23. Reich EE, Markesbery WR, Roberts LJ, 2nd, Swift LL, Morrow JD and Montine TJ (2001) Brain regional quantification of F-ring and D-/E-ring isoprostanes and neuroprostanes in Alzheimer's disease. *Am J Pathol* **158**, 293–297.
24. Sayre LM, Zelasko DA, Harris PL, Perry G, Salomon RG and Smith MA (1997) 4-Hydroxynonenal-derived advanced lipid peroxidation end products are increased in Alzheimer's disease. *J Neurochem* **68**, 2092–2097.
25. Smith MA (1998) Alzheimer disease. *Int Rev Neurobiol* **42**, 1–54.
26. Tanaka T, Nishiyama Y, Okada K, Hirota K, Matsui M, Yodoi J, Hiai H and Toyokuni S (1997) Induction and nuclear translocation of thioredoxin by oxidative damage in the mouse kidney: independence of tubular necrosis and sulfhydryl depletion. *Lab Invest* **77**, 145–155.
27. Uchida K and Stadtman ER (1992) Modification of histidine residues in proteins by reaction with 4-hydroxynonenal. *Proc Natl Acad Sci USA* **89**, 4544–4548.
28. Williams TI, Lynn BC, Markesbery WR and Lovell MA (2006) Increased levels of 4-hydroxynonenal and acrolein, neurotoxic markers of lipid peroxidation, in the brain in Mild Cognitive Impairment and early Alzheimer's disease. *Neurobiol Aging* **27**, 1094–1099.
29. Xiao Y, Huang Y and Chen ZY (2005) Distribution, depletion and recovery of docosahexaenoic acid are region-specific in rat brain. *Br J Nutr* **94**, 544–550.

Journal of Neuroscience Research

Journal of Neuroscience Research 88:798–806 (2010)

# Developmental and Age-Related Changes of Peptidylarginine Deiminase 2 in the Mouse Brain

Nobuko Shimada,[1] Setsuko Handa,[1] Yoshiaki Uchida,[2] Mitsugu Fukuda,[1] Naoki Maruyama,[1] Hiroaki Asaga,[3] Eun-Kyoung Choi,[4] Jaewon Lee,[5] and Akihito Ishigami[1,6]*

[1]Aging Regulation, Tokyo Metropolitan Institute of Gerontology, Tokyo, Japan
[2]Fujirebio, Inc., Tokyo, Japan
[3]Biological Science Laboratory, Meiji University, Tokyo, Japan
[4]Ilsong Institute of Life Science, Hallym University, Gyeonggi-do, Republic of Korea
[5]Department of Pharmacy, College of Pharmacy, Longevity Life Science and Technology Institute, Pusan National University, Busan, Republic of Korea
[6]Department of Biochemistry, Faculty of Pharmaceutical Sciences, Toho University, Chiba, Japan

Peptidylarginine deiminases (PADs) are a group of posttranslational modification enzymes that citrullinate (deiminate) protein arginine residues in a $Ca^{2+}$-dependent manner. Enzymatic citrullination abolishes positive charges of native protein molecules, inevitably causing significant alterations in their structure and functions. Among the five isoforms of PADs, PAD2 and PAD4 are proved occupants of the central nervous system (CNS), and especially PAD2 is a main PAD enzyme expressed in the CNS. We previously reported that abnormal protein citrullination by PAD2 has been closely associated with the pathogenesis of neurodegenerative disorders such as Alzheimer's disease and prion disease. Protein citrullination in these patients is thought to play a role during the initiation and/or progression of disease. However, the contribution of changes in PAD2 levels, and consequent citrullination, during developmental and aging processes remained unclear. Therefore, we used quantitative real-time RT-PCR, Western blot analysis, and immunohistochemical methods to measure PAD2 expression and localization in the brain during those processes. PAD2 mRNA expression was detected in the brains of mice as early as embryonic day 15, and its expression in cerebral cortex, hippocampus, and cerebellum increased significantly as the animals aged from 3 to 30 months old. No citrullinated proteins were detected during that period. Moreover, we found here, for the first time, that PAD2 localized specifically in the neuronal cells of the cerebral cortex and Purkinje cells of the cerebellum. These findings indicate that, despite PAD2's normally inactive status, it becomes active and citrullinates cellular proteins, but only when the intracellular $Ca^{2+}$ balance is upset during neurodegenerative changes. © 2009 Wiley-Liss, Inc.

Key words: cerebellum; citrullination; neurodegenerative disorder; PAD2; Purkinje cells



Because concentrations of peptidylarginine deiminases (PADs; EC 3.5.3.15) become altered during developmental and aging processes and have been linked to abnormal accumulations of citrullinated proteins in degenerative diseases of the brain, we sought to establish in detail the levels and impact of PADs in neonatal and aging mice. PADs are posttranslational modification enzymes that citrullinate (deiminate) protein arginine residues in a calcium ion-dependent manner, yielding citrulline residues (Watanabe et al., 1988; Vossenaar et al., 2003). Enzymatic citrullination abolishes positive charges of native protein molecules, thereby altering their structure and functions over time (Tarcsa et al., 1996). Although the five isoforms of PADs (i.e., types 1, 2, 3, 4/5, and 6) reside in multiple mammalian tissues (Watanabe et al., 1988; Vossenaar et al., 2003), their tissue-specific expression differs according to analysis by reverse transcriptase-polymerase chain reaction (RT-PCR; Ishigami et al., 2001). However, all these isoforms display nearly identical amino acid sequences (Ishigami et al., 2002). Among them, PAD2 and PAD4 occupy the central nervous system (CNS), and especially PAD2 is a main PAD enzyme expressed in the CNS.

These isoforms are present in myelin sheath, and hypercitrullination of myelin basic protein (MBP) resulted in loss of myelin sheath integrity in multiple sclerosis (MS)

The first two authors contributed equally to this work.

Contract grant sponsor: Ministry of Education, Science, and Culture, Japan (to N.S., A.I.).

*Correspondence to: Akihito Ishigami, PhD, Department of Biochemistry, Faculty of Pharmaceutical Sciences, Toho University, Miyama 2-2-1, Funabashi, Chiba 274-8510, Japan. E-mail: ishigami@phar.toho-u.ac.jp

Received 10 April 2009; Revised 20 July 2009; Accepted 24 July 2009

Published online 14 October 2009 in Wiley InterScience (www.interscience.wiley.com). DOI: 10.1002/jnr.22255

patients (Moscarello et al., 1994; Musse et al., 2008; Wood et al., 2008). Moreover, PAD4, the nuclear isoform of this family of enzymes, is involved in histone citrullination in the MS brain (Mastronardi et al., 2006). Immunocytochemical studies have localized PAD2 in glial cells, especially astrocytes (Asaga and Ishigami, 2000, 2001), microglial cells (Asaga et al., 2002), and oligodendrocytes (Akiyama et al., 1999). Additionally, PAD2 expression was later detected in cultured Schwann cells (Keilhoff et al., 2008). However, although the presence of PAD2 in glial cells should have imbued them with citrullinated proteins, such proteins were rarely identified in those cells examined with our sensitive detection method (Senshu et al., 1992). Therefore, we assumed that PAD2 is normally inactive (Asaga and Ishigami, 2000, 2001; Asaga et al., 2002). However, under abnormal conditions, glial fibrillary acidic protein (GFAP) was highly susceptible to the attack of PAD2 in excised rat brains deliberately left at room temperature (Asaga and Senshu, 1993). Under hypoxic conditions (Asaga and Ishigami, 2000) and during kainic acid-evoked neurodegeneration (Asaga and Ishigami, 2001; Asaga et al., 2002), PAD2 became activated in regions undergoing neurodegeneration and functioned to citrullinate various cerebral proteins, indicating the involvement of protein citrullination in neurodegenerative processes. These findings provided an important clue; that is, PAD2 normally remains inactive but becomes active and citrullinates cellular proteins only when the intracellular calcium balance is upset during neurodegenerative changes. In fact, our previous report indicated that citrullinated proteins including GFAP, vimentin, and myelin basic protein (MBP) accumulated to an abnormal extent in the Alzheimer's disease (AD)-afflicted hippocampus and that the expression of PAD2 increased during related neurodegenerative changes (Ishigami et al., 2005). We subsequently described increases of the citrullinated proteins GFAP, MBP, enolases, and aldolases in the brains of mice infected with scrapie as a model of prion disease along with the increased expression and activity of PAD2, suggesting that accumulated citrullinated proteins and abnormal activation of PAD2 may play a role in the pathogenesis of prion diseases. Moreover, in patients with MS, citrullinated MBP was increased to 45% of total MBP compared with much smaller amounts in healthy adults (Moscarello et al., 1994) and was later regarded as a pathological mechanism of MS (Moscarello et al., 2007).

Because PAD2 activation and accumulation of citrullinated proteins in the brain are increasingly associated with the progression of neurodegenerative disorders such as AD, prion disease, and MS, it is very important to clarify the expression and localization of PAD2 in the brain during the developmental and aging process. For comparison of PAD2 expression and characteristic localization, we used microtubule-associated protein 2 (MAP2) and neurofilament 3 (Nef3) as neuronal cell markers and GFAP as a marker of astrocyte in this study. After applying quantitative real-time RT-PCR, Western blot analysis, and immunohistochemical methods, we found that PAD2 mRNA expression levels increased significantly in the cerebral cortex, hippocampus, and cerebellum during aging. Moreover, for the first time, PAD2 was identified in neuronal cells of the cerebral cortex and Purkinje cells of the cerebellum.

## MATERIALS AND METHODS

### Animals

Male C57BL/6 mice 3, 6, 12, 24, or 30 months of age were obtained from the Animal Facility at Tokyo Metropolitan Institute of Gerontology, and pregnant female mice were obtained from Japan SLC (Shizuoka, Japan). Mice at the embryonic days 15, 16, 17, and 18; postnatal days 1, 2, 3, 7, and 30; and ages 3, 6, 12, 24, and 30 months were used in this study. Throughout the experiments, animals were maintained on 12-hr light/dark cycles in a controlled environment. All experimental procedures using laboratory animals were approved by the Animal Care and Use Committee of Tokyo Metropolitan Institute of Gerontology.

### Brain Sample Preparation

Mice were anesthetized and systemically perfused with phosphate-buffered saline to wash out blood cells. Their brains were quickly excised and divided into cerebral cortex, hippocampus, and cerebellum. Brain sections were homogenized in 10 mM Tris-HCl (pH 7.6) containing 1 mM phenylmethylsulfonyl fluoride and centrifuged at 21,000*g* for 10 min at 4°C. For Western blot analysis, the supernatants were boiled for 5 min with a lysis buffer containing 0.125 M Tris-HCl (pH 6.8), 4% SDS, 20% glycerol, 10% 2-mercaptoethanol, and 0.2% bromophenol blue in a ratio of 1:1 and kept at −80°C until use. The protein concentration was determined by BCA protein assay (Pierce Biotechnology, Rockford, IL) using bovine serum albumin as a standard. To prepare total RNA, the brain sections were immediately frozen in liquid nitrogen and stored at −80°C until use. For immunohistochemical staining, brain tissues were immersed in 10% formalin (Wako Pure Chemical, Osaka, Japan) and left standing for 48 hr. Each fixed brain was cut in half laterally, then embedded in paraffin, and finally cut serially into 6-μm-thick cryosections. Human brain samples were obtained from the Brain Bank for Aging Research (BBAR) organized by the Tokyo Metropolitan Geriatric Hospital and Tokyo Metropolitan Institute of Gerontology (TMIG). Human studies were approved by the Ethics Committees of the TMIG.

### PAD2 Monoclonal Antibody

The entire coding sequence of human PAD2 (hPAD2; GenBank AB030176) was amplified by PCR using primers, pENTR-hPAD2 forward primer 5′-CACCATGCTGCGCGAGCGGACCGTGCGGCTG-3′ and pENTR-hPAD2 reverse primer 5′-CCGGAATTCGCGGCCGCTCTGGGCGTGTGAGGGAGGGTCTGGAG-3′. The PCR products were subcloned in pENTR/D-TOPO vector (Invitrogen, Carlsbad, CA). To produce N-terminal 6× his-tagged hPAD2-recombinant protein, hPAD2 cDNA was subcloned to pDEST17 vector (Invitrogen) and transformed with the BL21-AI strain of *Escherichia coli*. The transformants were grown overnight, then treated for 4 hr with 0.2% L-arabinose at 37°C. The bacteria were then disrupted by sonication, and the recombinant proteins were purified by using Ni-NTA

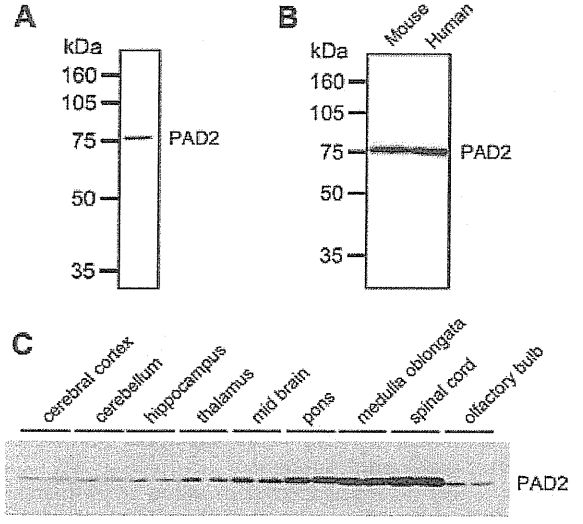


Fig. 1. Characterization of the anti-hPAD2 monoclonal antibody hPAD2-2110 and distribution of PAD2 protein in the CNS. **A:** Purified recombinant hPAD2 protein was separated on 10% SDS-PAGE, followed by Coomassie brilliant blue staining. **B:** Mouse and human brain samples were prepared as described in Materials and Methods. Ten micrograms of extracted proteins were separated on 10% SDS-PAGE and then electrotransferred onto a PVDF membrane. PAD2 was detected by using anti-hPAD2 monoclonal antibody. **C:** Under the stereoscopic microscope, each brain from 3-month-old mice was divided into nine parts: the cerebral cortex, cerebellum, hippocampus, thalamus, midbrain, pons, medulla oblongata, spinal cord, and olfactory bulb. From each part, 10 μg of extracted proteins was separated on 10% SDS-PAGE. PAD2 was detected by using anti-hPAD2 monoclonal antibody. Analyses were performed in duplicate with samples from two individual mice.

agarose beads (Qiagen, Valencia, CA). The identity of recombinant hPAD2 proteins was verified by sodium dodecyl sulfate (SDS)- polyacrylamide gel electrophoresis (PAGE), followed by Coomassie brilliant blue staining (see Fig. 1A).

Purified recombinant hPAD2 (50 μg) in complete Freund's adjuvant was injected into BALB/c mice, which were then given a booster injection of the same antigen in incomplete Freund's adjuvant. Three days after the last injection, spleen cells were fused with mouse P3U1 myeloma cells by using polyethylene glycol, and fused cells were cultured with HAT medium (Invitrogen). The specificities of hPAD2 monoclonal antibody-producing cells, hPAD2-264, hPAD2-2110, hPAD2-2111, hPAD2-2147, hPAD2-2153, hPAD2-2167 clones, were determined by enzyme-linked immunosorbent assays and Western blot analysis. Only the anti-hPAD2 monoclonal antibody hPAD2-2110 was purified from ascites by protein G Sepharose 4 Fast Flow columns (GE Healthcare, Piscataway, NJ). Anti-hPAD2 monoclonal antibody hPAD2-2110 reacted with both human and mouse PAD2 in the brain as confirmed by Western blot analysis (Fig. 1B).

### Western Blot Analysis

Equal amounts of protein (10 μg/lane) were separated by SDS-PAGE on vertical slab 10% polyacrylamide gels (1 mm × 9 cm) by the method of Laemmli (1970). Proteins were then electrophoretically transferred from polyacrylamide gels onto a membrane of poylvinylidene difluoride (PVDF; Millipore, Billerica, MA) by the method of Towbin et al. (1979). The membrane was then incubated successively with anti-hPAD2 monoclonal antibody (hPAD2-2110; 1:1,000) and horseradish peroxidase-labeled goat anti-mouse IgG (Bio-Rad, Hercules, CA). Chemiluminescence signals were detected with a LAS-3000 imaging system (Fujifilm, Tokyo, Japan) using ECL Western Blotting Detection Reagents (GE Healthcare UK Ltd. Amersham, Little Chalfont, Buckinghamshire, United Kingdom). Signal intensity was analyzed by using Multi Gauge software (Fujifilm).

### RT-PCR

Total RNA was extracted by using Isogen (Wako Pure Chemical, Osaka, Japan). Brain samples were homogenized with a Teflon-pestle homogenizer in Isogen, and total RNA was extracted according to the supplier's instructions. The final RNA pellet was dissolved in diethyl pyrocarbonate-treated $H_2O$, and the RNA concentration was determined and confirmed to be free from protein contamination by measuring absorbance at 260 and 280 nm. Five micrograms of total RNA from each sample was treated with Turbo DNase I (Ambion, Austin, TX) to eliminate any trace of genomic DNA. RT-PCR was performed with a Takara mRNA Selective PCR Kit (Takara, Kyoto, Japan) according to the supplier's instructions. Reverse transcription was performed with antisense oligonucleotide primers. Mouse PAD2 primers were designed in the 3′ noncording region of the cDNA after checking the absence of homology with any other PAD sequences by using the Blast program. The sense and antisense primers used were, for mouse PAD2, 5′-CTGCGG TCTCTGGGTCCTTCCTGTA-3′ and 5′-GACCAGGC-GAGAGAACAGAAATAGC-3′ (expected size 665 bp; Watanabe and Senshu, 1989); for mouse GFAP, 5′-CTGGAGG TGGAGAGGGACAACTT-3′ and 5′-CCGCATCTCCA-CAGTCTTTACCA-3′ (expected size 840 bp; Balcarek and Cowan, 1985); for mouse MAP2, 5′-GTGAACAAGA-GAAGGAAGCCCAACA-3′ and 5′-GGACCTGCTTGGG-GACTGTGTGATG-3′ (expected size 956 bp; Lewis et al., 1988); and, for mouse glyceraldehyde-3-phosphate dehydrogenase (GAPDH), 5′-GTGAAGGTCGGTGTGAACGGAT-3′ and 5′-GCCGCCTGCTTCACCACCTTCTT-3′ (expected size 788 bp; Tso et al., 1985). PCR conditions were 30 sec at 94°C, followed by 25, 30, or 40 cycles at 94°C for 30 sec, 60°C for 30 sec, and 72°C for 1 min, and a terminal extension period (72°C, 5 min). PCR products were visualized by gel electrophoresis in 1.2% agarose with ethidium bromide staining. To confirm their identity, PCR products were subcloned and sequenced.

### Quantitative Real-Time PCR Analysis

A final preparation of 1.8 μg for each total RNA was subjected to two-step quantitative real-time PCR. In the first step, reverse transcription reaction was carried out with a random primer and SuperScript II (Invitrogen) in the presence of RNase inhibitor. For the second step, synthesized cDNA was

applied to the inventoried TaqMan gene expression assay by using the real-time PCR equipment (Applied Biosystems 7300 Real Time PCR System; Applied Biosystems, Foster City, CA). For quantitative analysis, a standard curve method was designed using a common standard prepared by mixing an aliquot of all samples from the experiment, and the standard was diluted serially to compute the threshold cycle covering the range between 18 and 35. The samples were also diluted properly for each of the target genes and GAPDH to be measured on the linear range of the semilogarithmic standard curve. All assays were performed under the standard curve correlation factor above 0.990. Values of unknown samples were corrected for dilution factor and normalized to the GAPDH level assumed as a constant. The expression of PAD2, GFAP, and Nef3 was analyzed, and the results are shown as percentage value; i.e., the level at postnatal day 30 and hippocampus at 3-months-old was considered as 100%. All assays were performed in duplicate.

### Immunohistochemical Staining

After removal of paraffin, the brain sections were heated by microwave in 0.1 M citrate buffer (pH 7.0), followed by inactivation of endogenous peroxidase during incubation with 1% hydrogen peroxide in methanol. The primary antibodies used were mouse monoclonal PAD2 antibody (hPAD2-2110, 1:1,000), rabbit polyclonal GFAP antibody (1:1,000; Cosmo Bio, Tokyo, Japan), and mouse monoclonal MAP2 antibody (1:1,000; Chemicon, Temecula, CA). PAD2, GFAP, and MAP2 were detected by indirect immunoperoxidase staining using corresponding Histofine Simple Stain MAX-PO kits (Nichirei Biosciences, Tokyo, Japan) and 3,3′-diaminobenzidine (DAB) as a chromogenic substrate. After DAB staining, nuclei were counterstained with Myer's hematoxylin.

For double staining of PAD2 and calbindin-D-28K (calbindin), rabbit anticalbindin antibody (Thermo Fisher Scientific, Fremont, CA) was reacted first, and the alkaline phosphatase-conjugated anti-rabbit IgG (Histofine; Nichirei Biosciences) was reacted to stain with a Red Alkaline Phosphate Substrate Kit I. Second, anti-PAD2 monoclonal antibody (hPAD2-2110) was reacted, then horseradish peroxidase-conjugated anti-mouse IgG was reacted to stain with DAB.

### Statistical Analysis

Results are expressed as mean ± SEM. The probability of statistical differences between experimental groups was determined by Bonferroni's multiple-comparisons test subsequent to one-way ANOVA. A statistical difference was considered significant at $P < 0.05$.

## RESULTS

### Distribution of PAD2 Protein in the CNS

We searched for PAD2 protein throughout the CNS by examining the cerebral cortex, cerebellum, hippocampus, thalamus, midbrain, pons, medulla oblongata, spinal cord, and olfactory bulb of 3-month-old mice. Western blot analysis revealed PAD2 protein in all these regions (Fig. 1C). Specifically, we calculated a ratio of PAD2 protein in the cerebellum, hippocampus, thalamus, midbrain, pons, medulla oblongata, spinal cord, and olfactory bulb compared with the amount of PAD2 protein in the cerebral cortex as 1.3-fold, 1.4-fold, 1.7-fold, 2.3-fold, 3.8-fold, 5.6-fold, 9.9-fold, and 1.6-fold, respectively.

### Developmental Change of PAD2 mRNA Expression Level in the Whole Brain

To assess our assumption that PAD2 mRNA expression levels undergo developmental changes, we examined whole brains of mice from embryonic day 15 to postnatal day 30 by both RT-PCR and quantitative real-time PCR. Small amounts of PAD2 mRNA were detected at 15 days of embryonic life and increased slightly until birth (Fig. 2A,B). After birth, the PAD2 mRNA level was constant until the third postnatal day and then significantly increased 2.5-fold at day 7 and 9.9-fold at day 30 compared with value at postnatal day 3 (Fig. 2B). Moreover, the PAD2 mRNA level at 30 days after birth was a statistically significant 3.9-fold higher than that at the seventh postnatal day. Similarly, amounts of PAD2 protein in the whole brain were small at embryonic day 16, held constant until the third postnatal day, then significantly increased to 5.9-fold at 7 days and to 17-fold at 30 days after birth compared with the amount of PAD2 protein at the third postnatal day (Western blot analysis; Fig. 3).

GFAP as a marker of astrocyte mRNA was detected at 16 days of embryonic life and increased until 3 postnatal days, then continued to increase until reaching a significant increment at the seventh and again at the thirtieth postnatal days (Fig. 2A,C). The GFAP mRNA level at 7 days and 30 days after birth also rose significantly to 3.4-fold and 2.4-fold higher levels than that at 3 days after birth (Fig. 2C). On the other hand, mRNAs for MAP2 and Nef3, the neuronal cell markers, were detectable in 15-day-old embryos and increased slightly until birth (Fig. 2A,D). The Nef3 mRNA level at 30 days of postnatal was a significant 1.3-fold higher than that at postnatal day 7 (Fig. 2D).

### Age-Related Change of PAD2 mRNA Expression Level

The age-related changes of PAD2, GFAP, and Nef3 mRNA in the cerebral cortex, cerebellum, and hippocampus of 3-month-old to 30-month-old mice were analyzed by quantitative real-time PCR. PAD2 mRNA expression was detected in the cerebral cortex, cerebellum, and hippocampus, but the cerebral cortex contained significantly less PAD2 mRNA than was found in the cerebellum and hippocampus regardless of the animals' ages (Fig. 4A). Moreover, PAD2 mRNA levels at all three sites gradually increased during aging. PAD2 mRNA levels in the cerebral cortex, cerebellum, and hippocampus at 30 months were about 1.6-fold, 1.5-fold, and 1.6-fold higher, respectively, than in 3-month-old animals.

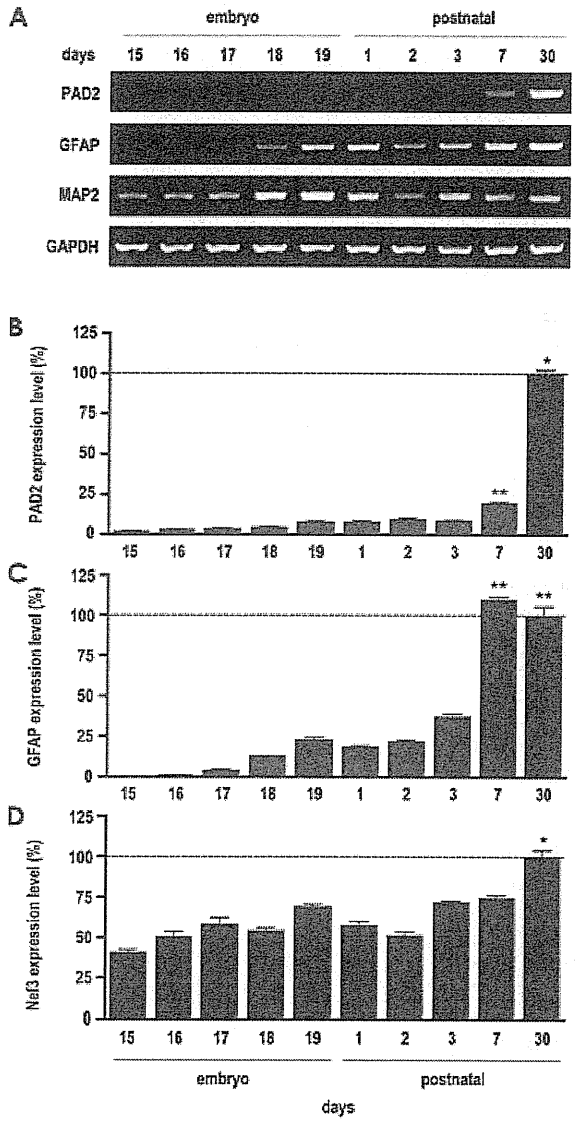


Fig. 2. Developmental changes of PAD2, GFAP, MAP2, and Nef3 mRNA expression levels in the whole brains of mice. **A:** RT-PCR was carried out with 1 μg of total RNA and specific oligonucleotide primer of PAD2, GFAP, MAP2, and GAPDH as described in Materials and Methods. An aliquot of each PCR product was electrophoresed in 1.2% agarose gel and stained with ethidium bromide for detection under UV light. **B–D:** Quantitative real-time PCR analysis was carried out with TaqMan primers and probes specific to PAD2 (B), GFAP (C), and Nef3 (D). As the endogenous control, GAPDH was quantified simultaneously and used to normalize each raw data point. Data from quantitative real-time PCR are shown as the percentage of each value, with postnatal day 30 taken as 100%, and represent mean ± SEM of five animals. $*P < 0.05$ compared with 15–19 days of embryonic life and 1–3 or 7 days after birth. $**P < 0.05$ compared with 15–19 days of embryonic life and 1–3 days after birth.

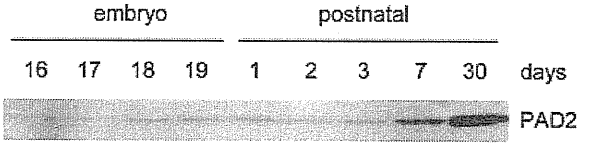


Fig. 3. Western blot analysis of PAD2 protein in the whole brain during development from embryonic day 16 to postnatal day 30. Ten micrograms of protein extracted from the whole brain was separated on 10% SDS-PAGE and then electrotransferred onto the PVDF membrane. PAD2 was detected by using anti-hPAD2 monoclonal antibody, hPAD2-2110.

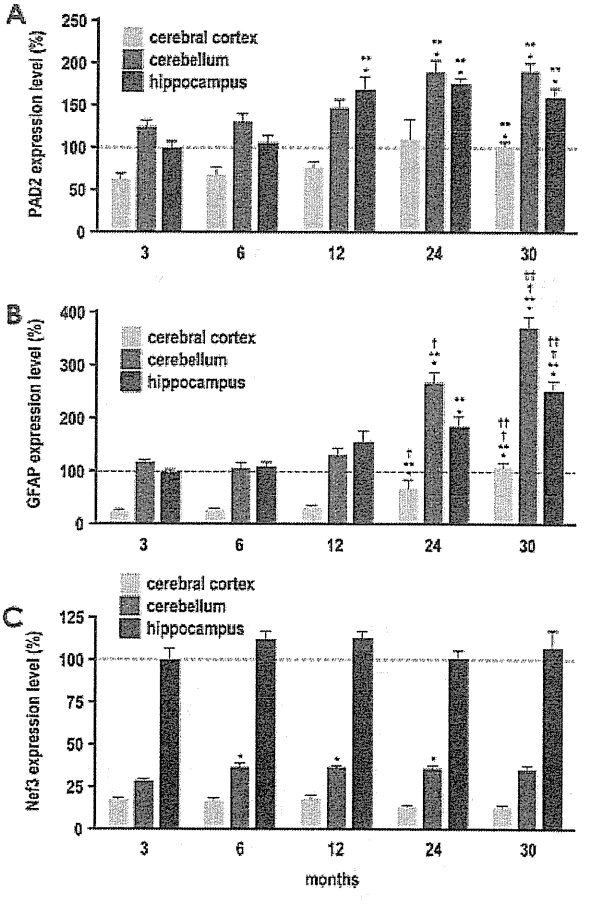


Fig. 4. Age-dependent changes of PAD2, GFAP, and Nef3 mRNA expression in the brain. Total RNA from the cerebral cortex, cerebellum, and hippocampus of 3-, 6-, 12-, 24-, and 30-month-old mice was prepared. Quantitative real-time PCR analysis of PAD2 (A), GFAP (B), and Nef3 (C) was carried out as described in Materials and Methods. As the endogenous control, GAPDH was quantified simultaneously to normalize each raw data. Data are expressed in percentages, with values in the hippocampus of 3-month-old mice taken as 100%, and represent a mean ± SEM of five animals. $*P < 0.05$ compared with 3-month-old mice. $**P < 0.05$ compared with 6-month-old mice. $^{\dagger}P < 0.05$ compared with 12-month-old mice. $\dagger\dagger P < 0.05$ compared with 24-month-old mice.

Similarly, GFAP mRNA expression in the cerebral cortex, cerebellum, and hippocampus gradually increased during aging, although the GFAP mRNA content in the cerebral cortex was significantly lower than that in the cerebellum and hippocampus at all ages (Fig. 4B). GFAP expression in the cerebral cortex, cerebellum, and hippocampus at 30 months was about 4.2-fold, 3.1-fold, and 2.5-fold higher than in 3 month-old-mice, respectively. On the other hand, Nef3 mRNA expression was detected in the cerebral cortex, cerebellum, and hippocampus and was abundantly expressed in the hippocampus of mice at all ages tested. Moreover, Nef3 mRNA expression levels in all regions did not change during aging (Fig. 4C).

### Immunohistochemical Localization of PAD2 in the Cerebral Cortex, Cerebellum, and Hippocampus

To establish firmly that PAD2-positive cells are present in the cerebral cortex, hippocampus, and cerebellum of 3-month-old mice, we performed immunohistochemical staining of serial sections by using PAD2-, GFAP-, and MAP2-specific antibody (Fig. 5). In the cerebral cortex and hippocampus, PAD2-positive signals were detected in neuronal cell bodies that costained with MAP2 (Fig. 5G,H,M,N) but not in dendrites. Not only was MAP2 staining positive in both the neuronal cell bodies and the dendrites, but the cerebral cortex, hippocampus, and cerebellum were also MAP2-positive (Fig 5M–O). However, GFAP-positive cells, which are considered to be reactive astrocytes, were PAD2 negative in the cerebral cortex, hippocampus, and cerebellum (Fig. 5G–L).

In the cerebellum, PAD2-positive staining was present on morphologically characteristic Purkinje-like cells along dense granule cell layers that were not positive for either MAP2 or GAFP (Fig. 5I,L,O). To confirm that these were actually Purkinje cells, we performed double immunostaining with PAD2 and calbindin, a known marker of Purkinje cells and limited to localization in those cells (Servais et al., 2005; Whitney et al., 2008; Fig. 6). Calbindin staining was evident as a light magenta coloration on the alkaline phosphate substrate (Fig. 6A). These Purkinje cells appeared as huge, round cell bodies located between the bottom of the molecule layer and surface of the granule cell layer of cerebellar tissue. PAD2 was stained brown by the DAB used as a chromogenic substrate (Fig. 6B). Double immunostaining allowed detection of both calbindin- and PAD2-positive cells in the same Purkinje cells from the cerebellum (Fig. 6C), thus ensuring the existence of PAD2 in clearly identified Purkinje cells of the cerebellum. Additionally, the characteristic localization of PAD2, GFAP, and MAP2 in the cerebral cortex, hippocampus, and cerebellum did not change during aging from 3 months to 30 months (data not shown).

## DISCUSSION

We report here, for the first time, that PAD2 mRNA expression increases significantly in the cerebral cortex, hippocampus, and cerebellum during aging and that PAD2 localizes in neuronal cells of the cerebral cortex and Purkinje cells of cerebellum. Activation of the PAD2 enzyme is a known cause of protein citrullination (Watanabe et al., 1988; Vossenaar et al., 2003). The potential clinical importance of the findings presented here lies in the close association previously found between abnormal protein citrullination in the CNS and the neurodegenerative disorders AD (Ishigami et al., 2005), MS (Moscarello et al., 2007) and prion disease (Jang et al., 2008). However, until now, changes of PAD2 expression levels have not been linked with the aging process.

In this study, PAD2 mRNA expression was detected in the brains of mice after 15 days of embryonic development, and GFAP mRNA expression first became evident just 1 day later (Fig. 1B,C). Previous reports indicated that PAD2 appeared mainly in glial cells, especially astrocytes (Asaga and Ishigami, 2000, 2001), microglial cells (Asaga et al., 2002), and oligodendrocytes (Akiyama et al., 1999). However, we detected PAD2 earlier than GFAP, so PAD2 must be expressed in cells other than glial cells, possibly astrocytes. MAP2 and Nef3 were also expressed at an early embryonic stage in amounts that increased slightly until birth and remained almost constant until postnatal day 7 (Fig. 2A,D). Thus, PAD2 expression did not correlate with GFAP, MAP2, or Nef3 expression, indicating that PAD2 must appear at specific, but still unknown, stages and conditions of glial and neuronal cell differentiation.

In the cerebral cortex, cerebellum, and hippocampus, PAD2 mRNA expression increased significantly during the aging process (Fig. 4A). That is, PAD2 mRNA levels at the 30-month-old mark were 1.5-fold to 1.6-fold higher than in 3 month olds. Although GFAP mRNA expression also increased significantly during aging, the increase of GFAP did not correlate closely with that of PAD2, because GFAP in 30-month-old mice was 2.7-fold to 4.7-fold higher than that from 3 month olds, far exceeding the increase of PAD2. Moreover Nef3 mRNA expression did not change during aging. Because the change of PAD2 expression levels during aging did not correlate with those of GFAP and Nef3, PAD2 must be expressed only at certain times and under appropriate conditions by neuronal cells and glial cells, including astrocytes (Asaga and Ishigami, 2000, 2001), activated microglial cells (Asaga et al., 2002), and stage-specific immature oligodendrocytes (Akiyama et al., 1999).

Wood et al. (2008) reported that both PAD2 and PAD4 isoforms were present in myelin isolated from normal and MS white matter, and PAD4 was involved in histone citrullination in MS brain (Mastronardi et al., 2006). However, in this study, PAD4 protein was not detected at all by Western blot analysis with the PAD4-specific antibody we developed previously (Nakashima

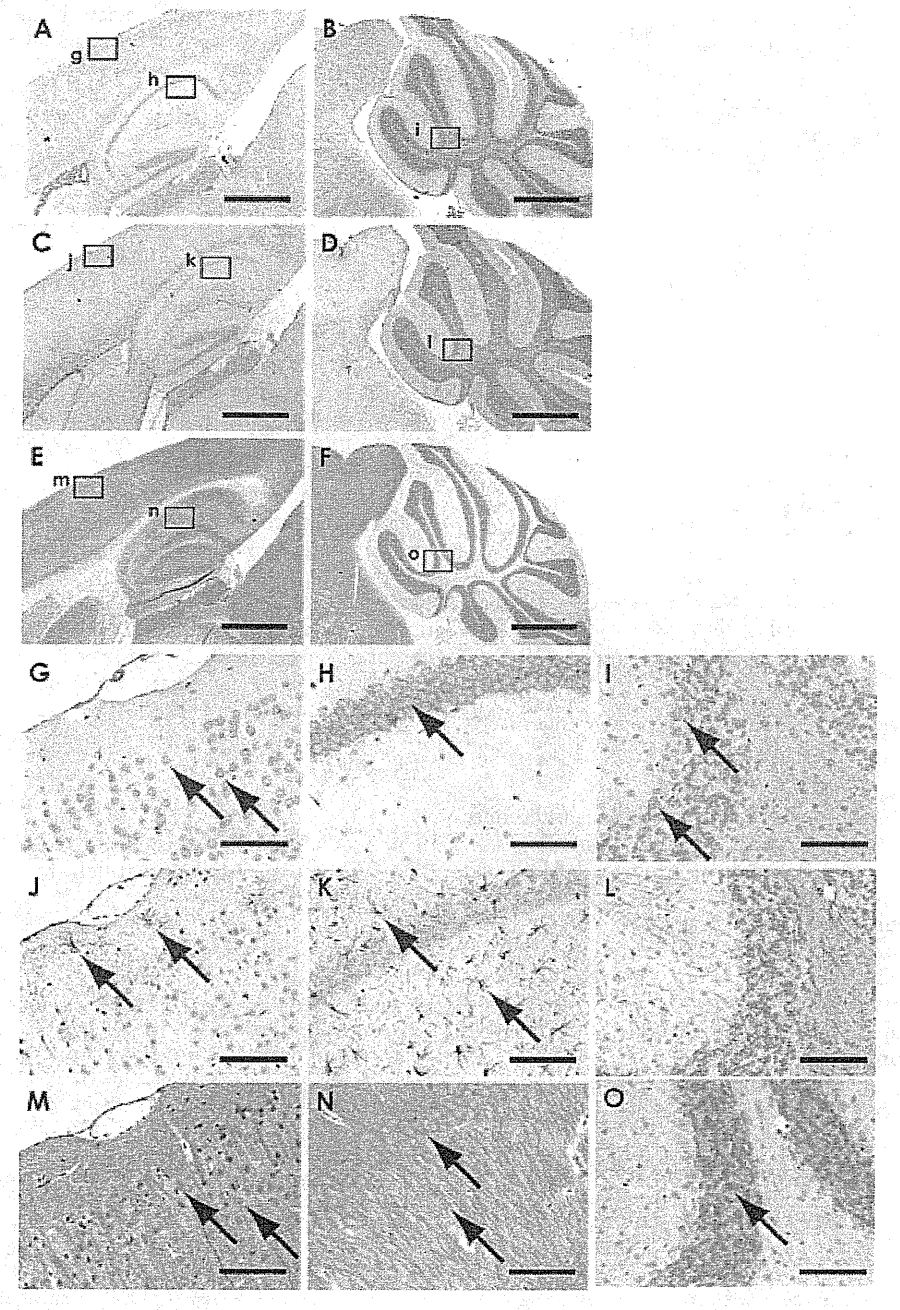


Fig. 5. Immunohistochemical staining of PAD2, GFAP, and MAP2 in the cerebral cortex, hippocampus, and cerebellum of 3-month-old mice. Each brain section was stained with PAD2 (**A,B,G–I**), GFAP (**C,D,J–L**), and MAP2 (**E,F,M–O**) antibody. The square area of g–i in A and B, j–l in C and D, and m–o in E and F were magnified for presentation in G–I, J–L, and M–O, respectively. Arrows indicate typical stained objects. Scale bars = 1 mm in A–F; 100 μm in G–O. [Color figure can be viewed in the online issue, which is available at www.interscience.wiley.com.]

et al., 1999). This discrepancy must be due to the different antibodies used. Moscarello et al. (1994) reported that approximately 20% of the total MBP was citrullinated in early developing human brain determined by protein sequencing; however, in this study, no citrullinated protein at all was found in the brain during normal development and aging by Western blot analysis with antimodified citrulline antibody (Senshu et al., 1992).

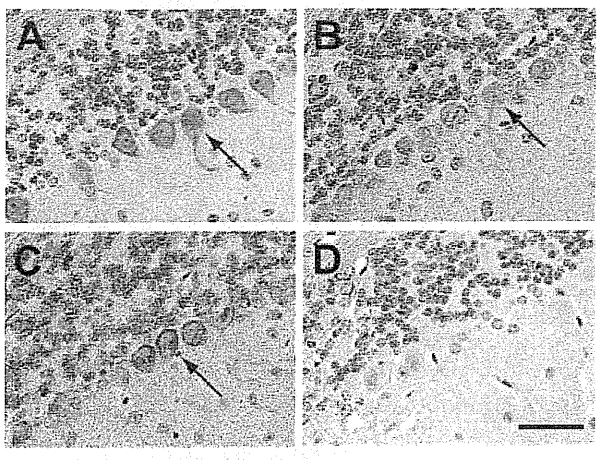


Fig. 6. Identification of PAD2-positive cells in the cerebellum by double immunostaining. Sections of cerebellum from 3-month-old mice were double immunostained with PAD2 and calbindin. Rabbit anticalbindin antibody was applied first, after which alkaline phosphatase-conjugated anti-rabbit IgG was applied for staining with the Red Alkaline Phosphate Substrate Kit I. Next, anti-PAD2 monoclonal antibody (hPAD2-2110) was applied; then, horseradish peroxidase-conjugated anti-mouse IgG was added to stain with DAB. The stained proteins are the following. **A:** Alkaline phosphate substrate as a chromogenic substrate (light magenta) for calbin. [Color figure can be viewed in the online issue, which is available at www.interscience.wiley.com.]

This discrepancy must be due to the technical differences between protein sequencing and Western blot analysis.

As described in our previous reports, PAD2 was detected in activated astrocytes in brains from AD and scrapie-infected mice (Ishigami et al., 2005; Jang et al., 2008). Many reports have, in fact, indicated that PAD2 normally remains inactive but becomes active and citrullinates cellular proteins only when the intracellular calcium balance is upset during neurodegenerative changes such as AD, prion disease, and MS (Moscarello et al., 1994; Ishigami et al., 2005; Jang et al., 2008). Thus, citrullinated protein has become a useful marker for neurodegenerative disorders of humans.

For the first time, PAD2 has been detected in Purkinje cells of the cerebellum, as we found by applying double-immunohistochemical staining for PAD2 and calbindin (Fig. 6). The cerebellum functions as the center of learning and control over motion, sensory input, and cognition. Purkinje cells of the cerebellum are its sole output neurons and are important as the integrators and fine tuners of diverse input signals (Cheron et al., 2008). Accumulated evidence indicates that the dynamic movement of $Ca^{2+}$ plays a key role in the function of Purkinje cells (Matsushita et al., 2002; Erickson et al., 2007). Intracellular $Ca^{2+}$ concentrations become elevated via voltage-dependent calcium channels of plasma membranes or inositol-1,4,5-triphosphate-dependent $Ca^{2+}$ release from intracellular $Ca^{2+}$ storage sites such as the endoplasmic reticulum (Cheron et al., 2008). Elevations of intracellular $Ca^{2+}$ activate an intracellular signal cascade leading to such functional events as neurotransmitter release (Cheron et al., 2008). The relevance of this background is that the PAD enzyme requires ~100-fold higher than the normal intracellular $Ca^{2+}$ level for its activation (Inagaki et al., 1989). Insofar as Purkinje cells store large amounts of $Ca^{2+}$ corresponding to physiological stimuli (Matsushita et al., 2002), conceivably those intracellular $Ca^{2+}$ concentrations become elevated transiently in specific, limited areas, such as near the endoplasmic reticulum and plasma membrane. When such a condition prevails, PAD2 enzyme would become activated and citrullinate various proteins, leading to cell death (Asaga et al., 1998). In fact, quantities of PAD2 and citrullinated proteins have been shown to increase in the brain in vivo during such abnormal conditions as scrapie-infection of mice and AD of humans (Ishigami et al., 2005; Jang et al., 2008).

In conclusion, we detected PAD2 mRNA in the brains of mice beginning at embryonic day 15 and tracked its ever-increasing expression in the cerebral cortex, hippocampus, and cerebellum until the animals were 30 months old. Moreover, we found here, for the first time, that PAD2 localized in neuronal cells of the cerebral cortex and Purkinje cells of the cerebellum. PAD2 may play a role in the onset and progression of neurodegenerative disorders by abnormally disrupting $Ca^{2+}$ homeostasis and thereby increasing the production of citrullinated proteins.

## ACKNOWLEDGMENT

We thank Ms. P. Minick for excellent editorial assistance.

## REFERENCES

Akiyama K, Sakurai Y, Asou H, Senshu T. 1999. Localization of peptidylarginine deiminase type II in a stage-specific immature oligodendrocyte from rat cerebral hemisphere. Neurosci Lett 274:53–55.

Asaga H, Ishigami A. 2000. Protein deimination in the rat brain: generation of citrulline-containing proteins in cerebrum perfused with oxygen-deprived media. Biomed Res 21:197–205.

Asaga H, Ishigami A. 2001. Protein deimination in the rat brain after kainate administration: citrulline-containing proteins as a novel marker of neurodegeneration. Neurosci Lett 299:5–8.

Asaga H, Senshu T. 1993. Combined biochemical and immunocytochemical analyses of postmortem protein deimination in the rat spinal cord. Cell Biol Int 17:525–532.

Asaga H, Yamada M, Senshu T. 1998. Selective deimination of vimentin in calcium ionophore-induced apoptosis of mouse peritoneal macrophages. Biochem Biophys Res Commun 243:641–646.

Asaga H, Akiyama K, Ohsawa T, Ishigami A. 2002. Increased and type II-specific expression of peptidylarginine deiminase in activated microglia but not hyperplastic astrocytes following kainic acid-evoked neurodegeneration in the rat brain. Neurosci Lett 326:129–132.

Balcarek JM, Cowan NJ. 1985. Structure of the mouse glial fibrillary acidic protein gene: implications for the evolution of the intermediate filament multigene family. Nucleic Acids Res 13:5527–5543.

Cheron G, Servais L, Dan B. 2008. Cerebellar network plasticity: from genes to fast oscillation. Neuroscience 153:1–19.

Erickson MA, Haburcak M, Smukler L, Dunlap K. 2007. Altered functional expression of Purkinje cell calcium channels precedes motor dysfunction in tottering mice. Neuroscience 150:547–555.

Inagaki M, Takahara H, Nishi Y, Sugawara K, Sato C. 1989. $Ca^{2+}$-dependent deimination-induced disassembly of intermediate filaments involves specific modification of the amino-terminal head domain. J Biol Chem 264:18119–18127.

Ishigami A, Asaga H, Ohsawa T, Akiyama K, Maruyama N. 2001. Peptidylarginine deiminase type I, type II, type III and type IV are expressed in rat epidermis. Biomed Res 22:63–65.

Ishigami A, Ohsawa T, Asaga H, Akiyama K, Kuramoto M, Maruyama N. 2002. Human peptidylarginine deiminase type II: molecular cloning, gene organization, and expression in human skin. Arch Biochem Biophys 407:25–31.

Ishigami A, Ohsawa T, Hiratsuka M, Taguchi H, Kobayashi S, Saito Y, Murayama S, Asaga H, Toda T, Kimura N, Maruyama N. 2005. Abnormal accumulation of citrullinated proteins catalyzed by peptidylarginine deiminase in hippocampal extracts from patients with Alzheimer's disease. J Neurosci Res 80:120–128.

Jang B, Kim E, Choi JK, Jin JK, Kim JI, Ishigami A, Maruyama N, Carp RI, Kim YS, Choi EK. 2008. Accumulation of citrullinated proteins by up-regulated peptidylarginine deiminase 2 in brains of scrapie-infected mice: a possible role in pathogenesis. Am J Pathol 173:1129–1142.

Keilhoff G, Prell T, Langnaese K, Mawrin C, Simon M, Fansa H, Nicholas AP. 2008. Expression pattern of peptidylarginine deiminase in rat and human Schwann cells. Dev Neurobiol 68:101–114.

Laemmli UK. 1970. Cleavage of structural proteins during the assembly of the head of bacteriophage T4. Nature 227:680–685.

Lewis SA, Wang DH, Cowan NJ. 1988. Microtubule-associated protein MAP2 shares a microtubule binding motif with tau protein. Science 242:936–939.

Mastronardi FG, Wood DD, Mei J, Raijmakers R, Tseveleki V, Dosch HM, Probert L, Casaccia-Bonnefil P, Moscarello MA. 2006. Increased citrullination of histone H3 in multiple sclerosis brain and animal models of demyelination: a role for tumor necrosis factor-induced peptidylarginine deiminase 4 translocation. J Neurosci 26:11387–11396.

Matsushita K, Wakamori M, Rhyu IJ, Arii T, Oda S, Mori Y, Imoto K. 2002. Bidirectional alterations in cerebellar synaptic transmission of tottering and rolling $Ca^{2+}$ channel mutant mice. J Neurosci 22:4388–4398.

Moscarello MA, Wood DD, Ackerley C, Boulias C. 1994. Myelin in multiple sclerosis is developmentally immature. J Clin Invest 94:146–154.

Moscarello MA, Mastronardi FG, Wood DD. 2007. The role of citrullinated proteins suggests a novel mechanism in the pathogenesis of multiple sclerosis. Neurochem Res 32:251–256.

Musse AA, Li Z, Ackerley CA, Bienzle D, Lei H, Poma R, Harauz G, Moscarello MA, Mastronardi FG. 2008. Peptidylarginine deiminase 2 (PAD2) overexpression in transgenic mice leads to myelin loss in the central nervous system. Dis Model Mech 1:229–240.

Nakashima K, Hagiwara T, Ishigami A, Nagata S, Asaga H, Kuramoto M, Senshu T, Yamada M. 1999. Molecular characterization of peptidylarginine deiminase in HL-60 cells induced by retinoic acid and 1α,25-dihydroxyvitamin $D_3$. J Biol Chem 274:27786–27792.

Senshu T, Sato T, Inoue T, Akiyama K, Asaga H. 1992. Detection of citrulline residues in deiminated proteins on polyvinylidene difluoride membrane. Anal Biochem 203:94–100.

Servais L, Bearzatto B, Schwaller B, Dumont M, De Saedeleer C, Dan B, Barski JJ, Schiffmann SN, Cheron G. 2005. Mono- and dual-frequency fast cerebellar oscillation in mice lacking parvalbumin and/or calbindin D-28k. Eur J Neurosci 22:861–870.

Tarcsa E, Marekov LN, Mei G, Melino G, Lee SC, Steinert PM. 1996. Protein unfolding by peptidylarginine deiminase. Substrate specificity and structural relationships of the natural substrates trichohyalin and filaggrin. J Biol Chem 271:30709–30716.

Towbin H, Staehelin T, Gordon J. 1979. Electrophoretic transfer of proteins from polyacrylamide gels to nitrocellulose sheets: procedure and some applications. Proc Natl Acad Sci U S A 76:4350–4354.

Tso JY, Sun XH, Kao TH, Reece KS, Wu R. 1985. Isolation and characterization of rat and human glyceraldehyde-3-phosphate dehydrogenase cDNAs: genomic complexity and molecular evolution of the gene. Nucleic Acids Res 13:2485–2502.

Vossenaar ER, Zendman AJ, van Venrooij WJ, Pruijn GJ. 2003. PAD, a growing family of citrullinating enzymes: genes, features and involvement in disease. Bioessays 25:1106–1118.

Watanabe K, Senshu T. 1989. Isolation and characterization of cDNA clones encoding rat skeletal muscle peptidylarginine deiminase. J Biol Chem 264:15255–15260.

Watanabe K, Akiyama K, Hikichi K, Ohtsuka R, Okuyama A, Senshu T. 1988. Combined biochemical and immunochemical comparison of peptidylarginine deiminases present in various tissues. Biochim Biophys Acta 966:375–383.

Whitney ER, Kemper TL, Bauman ML, Rosene DL, Blatt GJ. 2008. Cerebellar Purkinje cells are reduced in a subpopulation of autistic brains: a stereological experiment using calbindin-D28k. Cerebellum 7:406–416.

Wood DD, Ackerley CA, Brand B, Zhang L, Raijmakers R, Mastronardi FG, Moscarello MA. 2008. Myelin localization of peptidylarginine deiminases 2 and 4: comparison of PAD2 and PAD4 activities. Lab Invest 88:354–364.

# Over-expression of Senescence Marker Protein-30 Decreases Reactive Oxygen Species in Human Hepatic Carcinoma Hep G2 Cells

Setsuko HANDA,[a] Naoki MARUYAMA,[a] and Akihito ISHIGAMI*,[a,b]

[a] *Aging Regulation, Tokyo Metropolitan Institute of Gerontology; Tokyo 173–0015, Japan: and* [b] *Department of Biochemistry, Faculty of Pharmaceutical Sciences, Toho University; Chiba 274–8510, Japan.*
Received June 5, 2009; accepted July 18, 2009; published online July 24, 2009

**Senescence Marker Protein-30 (SMP30) is an androgen-independent factor that decreases with aging. We recently characterized SMP30 as a gluconolactonase (GNL) involved in the biosynthetic pathway of vitamin C and established that SMP30 knockout mice could not synthesize vitamin C *in vivo*. Although mice normally synthesize vitamin C, humans are prevented from doing so by mutations that have altered the gluconolactone oxidase gene during evolution. Even the SMP30/GNL present abundantly in the human liver does not synthesize vitamin C *in vivo*. To clarify the functions of this SMP30/GNL, we transfected the human SMP30/GNL gene into the human liver carcinoma cell line, Hep G2. The resulting Hep G2/SMP30 cells expressed approximately 10.9-fold more SMP30/GNL than Hep G2/pcDNA3 mock-transfected control cells. Examination of SMP30/GNL's impact on the state of oxidative stress in these cells revealed that formation of the reactive oxygen species (ROS) of mitochondrial and post-mitochondrial fractions from Hep G2/SMP30 cells decreased by a significant 24.0% and 18.1%, respectively, compared to those from Hep G2/pcDNA3 cells. Lipid peroxidation levels in Hep G2/SMP30 cells similarly decreased. Moreover, levels of the antioxidants superoxide dismutase (SOD) and glutathione (GSH) in Hep G2/SMP30 cells were a significant 42.6% and 62.4% lower than those in Hep G2/pcDNA3 cells, respectively. Thus, over-expression of SMP30/GNL in Hep G2 cells contributed to a decrease of ROS formation accompanied by decreases of lipid peroxidation, SOD activity and GSH levels.**

Key words senescence marker protein-30; gluconolactonase; reactive oxygen species; glutathione; superoxide dismutase

Senescence Marker Protein-30 (SMP30) was originally identified as a novel protein in the rat liver, the expression of which decreases androgen-independently with aging.[1,2] SMP30 is a 34 kDa protein expressed mainly in hepatocytes and renal tubular epithelia,[1] and its amino acid sequences are highly conserved among vertebrates, *i.e.*, 70 to 90%, strongly suggesting that the age-dependent decreases of SMP30 reported in the liver, kidney and lung may contribute to senescence.[1,3—7] SMP30 transcripts have been detected in multiple mouse tissues including the liver, kidney, brain, lung and testis by reverse transcription-polymerase chain reaction (RT-PCR) analysis.[7] In humans, immunohistochemical staining has localized SMP30 mainly in parenchymal cells of the liver, proximal tubular cells of the kidney, acinal and ductal cells of the pancreas and fasciculata cells of the adrenal cortex.[2] The human SMP30 gene, which is located in the p11.3–q11.2 segment of the X chromosome,[4] could be a candidate agent of X-linked diseases mapped to that region.

To clarify the physiological functions and the relationships between age-associated decreases of SMP30 and disorders of aged organs, we established SMP30 knockout mice.[8] These knockout animals are viable and fertile but lower in body weight and shorter in life span than the wild-type.[9] Throughout our experiments *in vitro* and *in vivo*, the livers of SMP30 knockout mice were far more susceptible to tumor necrosis factor (TNF)-$\alpha$- and Fas-mediated apoptosis than those from the wild-type.[8] Moreover, histological and biochemical analyses of livers from SMP30 knockout mice showed abnormal accumulations of neutral lipids and phospholipids.[9] This abnormal lipid metabolism must increase the tissues' susceptibility to apoptosis. Such changes of SMP30 expression might, then, account for the deterioration of cellular functions and lowered resistance to harmful stimuli in aged tissues.

We recently identified SMP30 as a gluconolactonase (GNL, EC 3.1.1.17) that is involved in the vitamin C biosynthetic pathway and found that SMP30/GNL knockout mice cannot synthesize vitamin C *in vivo*.[10] Humans, monkeys and guinea pigs are similarly incapable of synthesizing vitamin C *in vivo*, because the gluconolactone oxidase gene has mutated throughout evolution; however, mice, rats and many other animals do synthesize vitamin C *in vivo*. With aging, SMP30/GNL content decreases in the liver, kidney and lung, and such decreases affect the normally copious amount of SMP30/GNL in the livers of younger humans.[2] To discern what, if any, functions SMP30/GNL has in the human liver, we transfected the Hep G2 human liver carcinoma cell line with the human SMP30/GNL gene. In the present study, we found that the over-expression of SMP30/GNL in these Hep G2 cells contributed to the decrease of reactive oxygen species (ROS) formation, presumably increasing the cells' state of oxidative stress.

## MATERIALS AND METHODS

**Cell Culture** Stable transfectants expressing the human SMP30/GNL were established as described previously.[11] Briefly, a human hepatocellular carcinoma cell line, Hep G2,[12] was transfected with human SMP30/GNL cDNA[4] or, as a control, with pcDNA3 (Invitrogen, Carlsbad, CA, U.S.A.), which did not contain the human SMP30/GNL cDNA insert. A clone with a high level of human SMP30/GNL expression was selected and designated as Hep G2/SMP30. Control cells mock transfected with the pcDNA3 vector only were designated as Hep G2/pcDNA3. Cells were cultured in Dulbecco's modified Eagle's medium (DMEM) supplemented with 10% fetal calf serum, grown in 75 $cm^2$ plastic dishes at 37 °C in 5% $CO_2$ and air, and then subcultured weekly.

* To whom correspondence should be addressed. e-mail: ishigami@phar.toho-u.ac.jp

**Preparation of Mitochondrial and Post-mitochondrial Fractions** Cells were washed with ice-cold phosphate-buffered saline and harvested by scraping with a cell scraper in 50 mM phosphate buffer (pH 7.4) and complete protease inhibitor cocktail (Roche Applied Science, Indianapolis, IN, U.S.A.). Cells were homogenized and centrifuged at 600 *g* for 15 min to remove nuclear fractions. Supernatants were further centrifuged at 12000 *g* for 15 min; the mitochondrial fraction was then obtained from the precipitate and the post-mitochondrial fraction from the supernatant. The protein concentration of each fraction was determined with the BCA protein assay (Pierce Biotechnology, Inc., Rockford, IL, U.S.A.) using bovine serum albumin as a standard.

**Measurement of Reactive Oxygen Species (ROS)** The formation of ROS in mitochondrial and post-mitochondrial fractions of cells was measured by using Reactive Oxygen Species Detection reagents (Invitrogen, Carlsbad, CA, U.S.A.). Briefly, oxidation-sensitive carboxy-$H_2$DCFDA (C400) fluorescent dye was dissolved in dimethylsulfoxide at a concentration of 10 mM stock and kept at −80 °C in the dark. The solution was freshly diluted with 50 mM phosphate buffer (pH 7.4) to 50 $\mu$M before the experiment. Diluted C400 was added to mitochondrial and post-mitochondrial fractions (25 $\mu$g protein) in a 96-well plate to achieve a final concentration of 25 $\mu$M. The changes in fluorescence intensity were measured every 5 min from 0 to 60 min on a Fluorescence Plate Reader (Gemini EM, Molecular Devices, Sunnyvale, CA, U.S.A.) with excitation and emission wavelengths set at 485 and 530 nm, respectively. The changes of fluorescence intensity from 30 to 60 min were normalized by time and protein concentration and expressed as U/min/mg of protein.

**Western Blot Analysis** The amount of SMP30 expressed in cells was appraised by Western blot analysis as described previously.[11] Briefly, equal amounts of protein (10 $\mu$g) were separated by sodium dodecyl sulfate (SDS)-polyacrylamide gel electrophoresis (PAGE) on vertical slab gels containing 14% (w/v) acrylamide and 0.25% (w/v) *N,N'*-methylenebisacrylamide, by the method of Laemmli.[13] Proteins were then electrophoretically transferred from acrylamide gels onto a polyvinylidene fluoride (PVDF) membrane (Millipore, Bedford, MA, U.S.A.) by the method of Towbin *et al.*[14] The membrane was incubated successively with anti-rat SMP30/GNL antibody (1 : 5000)[8] and horseradish peroxidase-labeled goat anti-rabbit IgG (Bio-rad Laboratories, Richmond, CA, U.S.A.). Chemiluminescence signals were detected by LAS-3000 imaging system (FUJIFILM, Tokyo, Japan) using ECL™ Western Blotting Detection Reagents (Amersham Bioscience, Piscataway, NJ, U.S.A.).

**Determination of Lipid Peroxides** Lipid peroxidation was estimated by measuring thiobarbituric acid reactive substances (TBARS).[15] Cells grown in 75 $cm^2$ plastic dishes were washed with ice-cold phosphate-buffered saline, harvested by scraping with a cell scraper in 0.1% SDS and homogenized. 0.005 ml of 0.8% butylated hydroxytoluene, 0.02 ml of 8.1% SDS, 0.15 ml of citrate buffer (pH 3.5), 0.15 ml of 0.8% thiobarbituric acid solution and 0.07 ml of $H_2O$ were added to 0.01 ml of cell homogenate (10 $\mu$g protein) and pipetted into a tube. The mixture was incubated at 5 °C for 60 min and then heated in boiling water for 60 min. After cooling, the colored complex was extracted into 0.5 ml of *n*-butanol : pyridin (15 : 1), and the fluorescence intensity was measured on a Fluorescence Plate Reader (Gemini EM, Molecular Devices, Sunnyvale, CA, U.S.A.) with excitation and emission wavelengths set at 515 and 553 nm, respectively. The amount of lipid peroxides was calculated as TBARS products of lipid peroxidation and expressed as nmol malondialdehyde (MDA) per mg of protein.

**Superoxide Dismutase (SOD) Activity** SOD activity was measured using the SOD Assay Kit-WST (DOJINDO Laboratories, Kumamoto, Japan). Briefly, cells were homogenized in 50 mM phosphate buffer (pH 7.4) and complete protease inhibitor cocktail (Roche Applied Science, Indianapolis, IN, U.S.A.) and centrifuged at 10000 *g* for 15 min. This supernatant was used for determination of SOD enzyme activity according to the manufacturer's instructions.

**Determination of Glutathione (GSH)** Total GSH was determined using a Total Glutathione Quantification Kit (DOJINDO Laboratories, Kumamoto, Japan) according to the manufacturer's instructions. Briefly, cells were homogenized in 5% salicylsalicylic acid and centrifuged at 8000 *g* for 10 min. GSH levels in the supernatant were determined according to the manufacturer's protocol by measuring absorbance at 405 nm with an ELISA Plate Reader (Emax, Molecular Devices, Sunnyvale, CA, U.S.A.).

**Statistical Analysis** The results are expressed as means ± S.D. The probability of statistical differences between experimental groups was determined by unpaired Student's *t*-test. A statistical difference was considered significant at $p<0.05$.

## RESULTS

**Over-expression of Human SMP30/GNL in Transfectants of Hep G2 Cells** To clarify the physiological functions of SMP30/GNL in the human liver, we prepared Hep G2/SMP30 cells with a stable and abundant expression of human SMP30/GNL. Western blot analysis revealed that the amount of SMP30/GNL expressed in the Hep G2/SMP30 cells was 10.9-fold higher than that in Hep G2/pcDNA3 mock-transfected control cells (Fig. 1). Morphologically, the Hep G2/SMP30 and Hep G2/pcDNA3 cells were identical when examined by phase-contrast microscopy (data not shown).

**ROS Formation in Hep G2/SMP30 Cells** To examine the effect on ROS formation from over-expression of human SMP30/GNL in Hep G2 cells, the mitochondrial and post-mitochondrial fractions prepared from Hep G2/SMP30 and Hep G2/pcDNA3 cells were measured for ROS by using oxidation-sensitive C400 fluorescent dye. In both the mitochondrial and post-mitochondrial fractions from Hep G2/SMP30

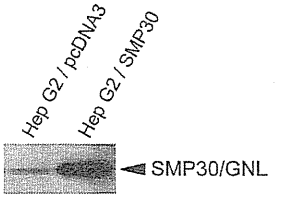


Fig. 1. Over-expression of Human SMP30/GNL in Hep G2/SMP30 Cells

10 $\mu$g of extracted proteins of Hep G2/SMP30 and Hep G2/pcDNA3 mock-transfected control cells were separated on 14% SDS-PAGE and then electro-transferred onto a PVDF membrane. SMP30/GNL was detected by using anti-rat SMP30 antibody. Arrow head indicates the human SMP30/GNL.